Low-invasive, wide-field, and cellular resolution two-photon imaging of neural population activity in brainstem and nucleus tractus solitarii

Authors:

Masakazu Agetsuma[1,2,3,*], Azumi Hatakeyama[3], Daisuke Yamada[3,4,*], Hiroshi Kuniishi[5], Eri Takeuchi[4], Shinji Tsuji[1], Chihiro Ito[2], Tomoko Kobayashi[1], Atsushi Noritake[6], Yoshitsugu Aoki[4], Hiroshi Yukawa[2], Akiyoshi Saitoh[3], Junichi Nabekura[1], Masayuki Sekiguchi[3,4,*]

Affiliations:

[1]Division of Homeostatic Development, National Institute for Physiological Sciences, 38 Nishigohnaka Myodaiji-cho, Okazaki, Aichi, 444-8585, Japan

[2] Quantum Regenerative and Biomedical Engineering Team, Institute for Quantum Life Science, National Institutes for Quantum Science and Technology (QST), Anagawa 4-9-1, Chiba Inage-ku, Chiba 263-8555, Japan

[3] Laboratory of Pharmacology, Faculty of Pharmaceutical Sciences, Tokyo University of Science, 2641 Yamazaki, Noda, Chiba 278-8510, Japan

[4]Department of Molecular Therapy, National Institute of Neuroscience, National Center of Neurology and Psychiatry, 4-1-1 Ogawahigashi, Kodaira, Tokyo 187-8502, Japan.

[5]Division of Development of Mental Functions, Research Center for Child Mental Development, University of Fukui, 23-3, Matsuokashimoaizuki, Eiheiji-cho, Yoshida-gun, Fukui 910-1193, Japan

[6]Division of Behavioral Development, Department of System Neuroscience, National Institute for Physiological Sciences, 38 Nishigohnaka Myodaiji-cho, Okazaki, Aichi, 444-8585, Japan

*Corresponding author. Email: age@nips.ac.jp, yamadada@rs.tus.ac.jp, and sekiguch@ncnp.go.jp

Keywords:
vagus nerve stimulation
two photon live brain imaging
nucleus tractus solitarii
brainstem
medulla oblongata

Summary: Brain-viscera communication is thought to play a crucial role in regulating mental health, with the vagus nerve being a key structure mediating this interaction. Clinically, artificial vagus nerve stimulation (VNS) is used to treat various neuropsychiatric disorders, highlighting the importance of vagal afferent fibers in regulating emotion. The nucleus tractus solitarii (NTS) is a brainstem structure proposed to receive direct signals from vagal afferents and relay them to the brain emotional regulatory networks. Direct evidence for this network is limited, however, due to the anatomic complexity and difficulty accessing the deep-brain NTS region in living animals. Here, to investigate this further, we developed a wide-field and deep-brain two-photon imaging method using a prism-based optical interface enabling the identification of cellular-resolution neural activities of the NTS while keeping the cerebellum, which covers the NTS, intact. This method allowed us to evaluate how NTS neurons respond to VNS and the gastrointestinal hormone cholecystokinin-8, suggesting its usefulness for investigating the role of the vagus-NTS pathway in regulating emotion.

Introduction

Regulating emotion through brain-viscera communication has received significant attention and abnormal communication is linked to neuropsychiatric disorders[1,2]. Brain-viscera communication occurs via neuronal and humoral mechanisms[3-6]. Neuronal pathways primarily involve the vagus nerve (10th cranial nerve), which comprises preganglionic efferent and afferent fibers. Preganglionic efferent fibers of the vagus nerve originate in the dorsal motor nucleus of the vagus nerve (10N, also known as DMNV or DMV) and the nucleus ambiguus in the brainstem. These fibers project to ganglia near their target organs and account for ~27% of vagal nerve fibers in the subdiaphragmatic trunk in rats[6]. Afferent fibers originating in the nodose ganglion in the cervical cord, comprising the remaining 73%, receive information from various internal organs and are proposed to relay it to the nucleus tractus solitarii (NTS)[6]. Efferent fibers regulate internal organ activity while afferent fibers relay organ condition information to the brain.

Artificial vagus nerve stimulation (VNS) is clinically applied for the treatment of various neurologic and psychiatric disorders[7,8]. Initially reported in the 19th century, the FDA approved VNS for treating drug-resistant seizures in 1997 and depression in 2005[9,10]. Currently, various neuropsychiatric and related disorders are considered potentially

treatable with VNS[11]. For safe and effective VNS, the parameter settings must be carefully optimized[12,13]. Research using rodent models is crucial for this optimization by elucidating the mechanisms underlying VNS and its therapeutic effects. Previous studies in rodents demonstrated that VNS effectively suppresses seizures[14,15], mitigates cerebral ischemia[16], and treats chronic pain[17]. Furthermore, VNS significantly reduces depressive symptoms[18,19] and aids in the extinction of associative fear memory[20]. These findings suggest that the insights gained from animal models are critical to advancing VNS-based clinical treatments and understanding the mechanisms of emotion regulation through the vagus nerve.

VNS is performed through an electrode targeting primarily afferent fibers of the left vagus nerve in the neck[21], with settings adjusted to minimize the activation of efferent fibers[22,23]. Although further research is required to confirm the direct connection, it is proposed that vagal afferent fibers project directly to neurons in the NTS[24]. Glutamate is believed to be the principal neurotransmitter released from vagal afferent terminals to the NTS, playing a key role in modulating respiration, cardiovascular reflexes, and gastrointestinal dynamics[25-30]. These findings suggest that the primary function of vagal nerve afferents is to activate NTS neurons. The NTS projects to various brain regions involved in emotion regulation, such as the amygdala, lateral hypothalamic area, bed nucleus of the stria terminalis, and periaqueductal gray[6,31]. In addition, VNS is hypothesized to regulate the activity of specific neuronal networks via the NTS[8] by (i) activating the thalamus and thalamocortical pathway, (ii) suppressing the amygdala and hippocampus, and (iii) increasing the release of noradrenaline and serotonin in widespread cerebral regions. Lesions of the locus coeruleus (LC), the primary origin of noradrenergic projections, suppress the anti-epileptic effects of VNS[14], indicating that these effects are mediated at least in part by the LC. Activity mapping using c-fos in rats reveals an increase in positive signals in the amygdala, cingulate, LC, and hypothalamus in response to VNS[32]. In humans, functional neuroimaging studies suggest that VNS causes long-term activity changes in the thalamus, cerebellum, orbitofrontal cortex, limbic system, hypothalamus, and medulla[33,34]. Together, these reports indicate that the vagus-NTS pathway is likely a critical gateway for VNS-based clinical treatments and for regulating emotions through brain-viscera communication.

The actual role of the NTS and the mechanisms underlying the therapeutic effects of

VNS, however, remain unclear. It is also unclear how information from the various organs relayed to the NTS is processed and whether the information is segregated or integrated at the NTS to regulate emotion. Addressing these questions has been challenging, however, because the NTS is located deep in the brain and is surrounded by regions critically involved in vital functions, making direct observation difficult. Although removing the cerebellum to expose the brainstem and allow for observations of a wide area of the brainstem, including the NTS, would enable more detailed studies of the information sent from the various organs involved in the digestive system[35], the cerebellum is also an essential brain structure for emotional regulation[36]. Therefore, the development of a novel technique for obtaining in vivo recordings of brainstem neurons that does not require removal of the cerebellum is in high demand. A technique to optically access the brainstem and NTS in the deep brain area while keeping the cerebellum intact would expand the possibilities for neural activity imaging and optogenetic neural activity manipulation, thereby profoundly advancing our understanding of the function of the NTS and its contribution to emotional regulation.

This aim motivated us to develop an in vivo two-photon imaging technique using a prism-based optical interface (Double-Prism based brainStem imaging under Cerebellar Architecture and Neural circuits, 'D-PSCAN'). The D-PSCAN method enables the observation of neural population activity with single-cell resolution in the brainstem and NTS situated deeply beneath the cerebellum while keeping the cerebellum and surrounding neural connections intact. We demonstrated the capability of this method to distinguish NTS activity from that of descending vagus neurons whose cell bodies lie ventrally to the NTS. The recorded neural activity data were used to evaluate the physiological characteristics of NTS neurons, i.e., their responsiveness to VNS. We also demonstrated the application of this imaging technique for detecting responsiveness to cholecystokinin-8 (CCK), a more physiologic stimulus than VNS. Our findings suggest the applicability of this method for future research on emotional regulation through the vagus-NTS pathway.

Results:

Double microprism for optical access to the brainstem area deep below the cerebellum

132 We developed a novel *in vivo* two-photon calcium imaging method for observing the
133 deep brain area in mice that enables neural population activity recordings in the brainstem
134 and NTS. Using a genetically encoded Ca^{2+} indicator, GCaMP, expressed by an adeno-
135 associated virus (AAV), we aimed to detect neural activities in the NTS (Figure 1A–B)
136 to observe the responsiveness of NTS neurons to various stimuli. Viruses encoding
137 GCaMP were injected into the NTS at approximately postnatal day (P) 50–60 for in vivo
138 imaging experiments, at least 1 month before the microprism implantation described
139 below. Although primarily targeted at the NTS, viruses often spread to adjacent areas,
140 beneficially inducing additional expression in surrounding regions and allowing us to
141 visualize wide areas of the brainstem.
142 The brainstem is located deeply below (2.0–2.5 mm) the dorsal surface of the
143 cerebellum. One potential problem in observing neural activities in the brainstem is that
144 even when the mouse head is fixed under the objective lens for two-photon imaging by
145 tightly attaching the head plate to the skull, the brainstem can still move somewhat
146 independently in response to the mouse's body movements[35]. Although standard skull
147 reference points (bregma and lambda) are typically referred to when targeting specific
148 brain areas, it is also crucial to visually capture the brain structure under observation in
149 each mouse. In a previous study, the cerebellum was removed to address these issues[35],
150 but the cerebellum is also involved in emotion control[36]; therefore, to accurately elucidate
151 the role of the vagus-NTS pathway in regulating emotion, it is essential to have a wide
152 field of view of the brainstem while keeping the cerebellum and neural connections intact.
153 To achieve this aim, we developed a technique to optically access the deep brainstem
154 area using a double prism (Figure 1C). We designed an implantable double microprism
155 assembly comprising a 2-mm right-angle glass microprism (TS N-BK7, 2 mm AL+MgF2,
156 Edmund) bonded to another 2-mm right-angle glass microprism and a 4 × 4 or 3 × 4 mm
157 cover glass window (No.1; Matsunami) at the surface-end position of the imaging
158 window. Dental cement was used to fix this assembly at the correct position for NTS
159 imaging. The cover glass enhanced adhesion to the dental cement, thereby securing the
160 position of the double microprism assembly and preventing dental cement from
161 obstructing its optical path. We implanted the assembly (simply termed 'double prism')
162 between the cerebellum and the brainstem using a custom-made vacuum-based
163 manipulator (Figure 1D and Figure S1A–B). To implant the double prism, the skull over

164 the dorsal surface of the cerebellum was carefully removed using a dental drill and fine
165 forceps (Figure S1C–D). A micro-knife was used to incise the thick dura mater between
166 the posterior edge of the cerebellum and the spinal cord. Removing the dura mater over
167 the cerebellum not only allows for smooth insertion of the prism but also adequately
168 relieves the pressure that might occur when the prism is inserted between the cerebellum
169 and brainstem.

170 Next, the newly developed vacuum-based prism holder was used to insert and implant
171 the double prism between the cerebellum and brainstem (Figure 1D–E, Figure S1B, E–
172 F). Sufficient space and no neural fibers remained between the cerebellum and brainstem
173 around the NTS area, enabling smooth insertion of the prism without cutting neural fibers.
174 Using a stereotaxic frame and vacuum-based prism holder attached to an equipped
175 manipulator, the prism can be precisely operated during the implantation while being
176 maintained in a horizontal position. The vacuum-based prism holder has a hook on one
177 side (Figure 1D and Figure S1A–B), which exerts a pushing force when sliding the sharp
178 corner of the double prism between the cerebellum and brainstem from the caudal side to
179 the rostral side (Figure 1D–E). After slowly inserting the double prism to approximately
180 1.6 mm deep, we waited a few minutes to ensure that breathing and other physical
181 conditions were not disturbed (Figure 1E). The double prism was slid further down at 0.1-
182 mm increments until reaching a maximum depth of 2.0 mm. Any physical reactions such
183 as disrupted breathing occurring during the insertion led us to promptly retract the prism.
184 Setting a stereomicroscope at an angle such that the brainstem can be visualized through
185 the double prism allows for clear observation of the arrangement of blood vessels in the
186 brainstem and fourth ventricle while inserting the prism.

187 After the double prism was fully inserted, UV craft resin was used to fix the double
188 prism and coat the surface of the targeted nerve structures (Figure S1F), followed by tight
189 fixation with dental cement. A resin coating was applied with the double prism remaining
190 in the holder and maintaining sufficient contact with the brainstem target area (including
191 the NTS) to prevent the resin from getting between them. After the UV resin had cured,
192 the holder was carefully released, and the double prism was firmly fixed to the
193 surrounding areas, including the remaining skull bone rostral to the cerebellum, using
194 dental cement. For further head fixation for two-photon imaging under the microscope
195 objective, the head plate was attached to the skull with dental cement (Figure 1F).

196 The double prism allows for optical access to the brainstem located on the ventral side
197 of the cerebellum, which exceeds 2.0 mm in thickness. Using the wide field of view and
198 horizontal coordinates, the position of the fourth ventricle serves as a key reference for
199 locating the NTS. Two-photon imaging through the double prism enabled us to detect
200 neural activities in the NTS at single-cell resolution, visualized by GCaMP (Figure 1G).
201 We named this method 'D-PSCAN'.
202 We confirmed the specificity of the method for detecting NTS neural activities. A
203 primary purpose for developing this imaging method was to investigate how information
204 from afferent vagus nerve inputs is processed in the NTS. On the other hand, the dorsal
205 motor nucleus (10N), where the cell bodies of the vagal efferent fibers originate, is located
206 just ventrally to the NTS[6], suggesting the importance of confirming specificity in the NTS
207 and distinguishing NTS neurons from 10N neurons. Importantly, the two-photon imaging
208 technique offers superior spatial resolution at depth. Based on this advantage, we
209 confirmed that the obtained signals originated from the brainstem surface area, i.e., the
210 NTS, rather than deeper regions such as 10N. To further test the specificity, we prepared
211 fixed brain slices after the in vivo imaging experiments and checked the expression of
212 GCaMP within the NTS. We used ChAT, an immunohistochemical marker, to identify
213 10N neurons[37] and distinguish NTS neurons histologically. Expression of GCaMP was
214 not observed in ChAT-positive cells within 10N (Figure 1B), indicating that NTS neuron
215 activities can be detected separately from efferent vagus neuron activities using this
216 method. We also checked for unanticipated retrograde labeling of the vagal afferent
217 terminals onto the NTS. Cell bodies of vagus neurons projecting to the NTS are located
218 in the nodose ganglion[6,38]. In mice that showed GCaMP expression in the NTS neurons,
219 we observed no GCaMP-expressing cell bodies in the nodose ganglion, i.e., vagus
220 sensory neurons (Figure S2). These findings demonstrated that, when imaging neural
221 activities around the NTS region using this method, we can distinguish activities of NTS
222 neurons from the signals of vagal afferent nerve terminals. Thus, the D-PSCAN method
223 enables us to specifically evaluate the activities of the NTS neurons separately from the
224 activities of vagal efferent neurons and vagal afferent fiber terminals.
225
226 <u>In vivo imaging of neural population activities at single-cell resolution in the brainstem</u>
227 <u>(NTS) of live mice</u>

228 Using the D-PSCAN method, we performed in vivo two-photon imaging and
229 recorded the neural population activities of the NTS and surrounding brainstem areas.
230 Spontaneous activities and stimulus-evoked responses of the brainstem neurons were
231 recorded by imaging GCaMP fluorescence changes (ΔF/F0). Brain motion artifacts
232 interfered with imaging in awake mice but were minimized under anesthesia, enabling
233 stable detection of the neural activities at a single-cell resolution both inside and outside
234 of the NTS area (Figure 2, Figure S3 and Supplementary Movie 1, 2). Time-lapse imaging
235 at various depths was performed by adjusting the imaging focal plane using a piezo to
236 move up and down in depth (Figure 2A and Figure S3). Volumetric live imaging (2 mm
237 x 2 mm horizontally, or smaller for zooming, 200–480 μm dorsoventrally, at 0.4–1.0 Hz
238 temporal resolution) of neural activities in the wide brainstem area (including the NTS)
239 of the head-fixed mouse was performed through the implanted double prism. Importantly,
240 this wide field of view and piezo-based volumetric imaging allowed us to detect GCaMP
241 fluorescence and neural activities not only from inside but also from outside of the NTS
242 areas and to confirm the specificity of the stimulus-evoked responses in the NTS, as
243 explained below.
244
245 Detection of single cell activities in the NTS as the direct efferent target of the vagus
246 nerve
247 To demonstrate the usefulness of the D-PSCAN for investigating the physiologic
248 characteristics of the NTS neurons, we applied the method to observe the neural responses
249 to artificial electrical stimulation of the afferent vagus nerve under various conditions
250 (vagus nerve stimulation, or VNS). We tested whether NTS neurons respond to the stimuli
251 and further evaluated the diversity of their responsiveness. To perform VNS, the bipolar
252 platinum hook electrode that has been used in rodents[39] was employed (Figure 2B). The
253 platinum hook electrode was surgically wrapped around the left vagus nerve of the mouse
254 and secured so that the positive and negative poles did not stick together. To create an
255 anodal block for the efferent direction, the cathode and anode were located on the rostral
256 and caudal sides, respectively, of the vagus nerve. The mechanism of the anodal block is
257 proposed to selectively bias activation toward vagal afferent fibers[22,23,40-42]. We
258 selectively targeted the left vagus nerve as left VNS elicits a greater afferent

259 response[22,23,43]. To keep the electrode position stable during in vivo NTS imaging, we
260 used silicone adhesive (Kwik-Sil™) to firmly secure the electrodes, and conducted
261 imaging experiments after closing the surgical wound.

262 We imaged the in vivo neural activity in the brainstem as VNS was repeatedly applied.
263 The VNS parameters were established based on previous studies, and various conditions
264 (i.e., various current intensities and stimulus frequencies) within the ranges reported in
265 prior rodent and human studies[12,22,23,44] were used to investigate the neural response
266 properties. Figure 2C presents an example in which the stimulation intensity was set to
267 1.0 mA and the stimulation frequency was 10 Hz. A pulse width of 100 microseconds
268 (μs) was consistently selected across all experiments in the present study. At a stimulus
269 frequency of 10 Hz, stimulation (100-μs current) occurred 10 times per second. The term
270 "trial" is defined as each 10-sec VNS duration, while the term "session" is defined as a
271 series of VNS trials at each condition (e.g., 1.0 mA at 10 Hz, 0.5 mA at 10 Hz, 1.0 mA at
272 5 Hz, etc.). In each session, the inter-trial interval was set at 50 sec. In the example case
273 shown in Figure 2, 10-sec VNS was repeated multiple times within a session to assess the
274 neural responses to each VNS condition.

275 Taking advantage of the 2 mm x 2 mm large field of view provided by the double
276 prism, we conducted volumetric observations of a wide brainstem area, including the NTS,
277 and compared neural responses to VNS inside and outside of the NTS (Figure 2D). In an
278 example case (Figure 2D), we measured a total of 16 z-planes at each time point. We
279 stacked every 4 consecutive plane from top to bottom to create an average image for each
280 time point. This stacking was done with a two-plane overlap; for instance, the first stack
281 included the 1st to 4th z-planes, the second stack included the 3rd to 6th z-planes, and
282 subsequent stacks followed this pattern. As a result, we obtained 7 stacked planes in total
283 in this experiment, labeled Zp1 through Zp7, respectively. This procedure is
284 advantageous to enhance the signal to noise ratio in each movie, which is critical for
285 further automatic detection of the active neurons[45]. After automatic detection of the active
286 neurons, we checked the existence of overlapped detection of the regions of interest (ROIs,
287 i.e., active neurons) between adjacent Zps, and removed such overlaps by manual
288 inspection.

289 Temporal dynamics of neural activity were clearly observed within the field of view
290 at multiple depths (Figure 2D and Supplementary Movie 1). Here, we present the baseline
291 GCaMP signal level (median fluorescence intensity) at Zp1, Zp2, and Zp4. NTS neurons
292 exhibiting stimulus-evoked and/or spontaneous neural activity were automatically
293 identified, and representative neurons are shown in the graph. In the case of neurons
294 outside of the NTS, we observed no clear responses to VNS and detected only
295 spontaneous (stimulus-independent) activities (neurons #1 and #2 in Figure 2D). On the
296 other hand, we detected a large number of neurons responding to VNS in the NTS area
297 (neurons #3–#21).
298 Two-photon imaging utilizes a scanning-type observation system, enabling seamless
299 transition from wide-field to high-magnification imaging using a single objective lens.
300 Depending on the point spread function of the objective lens, this approach facilitates the
301 acquisition of images with enhanced spatial resolution compared with maximum wide-
302 field imaging. Using this mechanism, after confirming the position of the NTS in the wide
303 field of view, we narrowed down the imaging area to the NTS and observed the neural
304 activities at high magnification (Figure 2E and Supplementary Movie 2). We detected
305 individual neuron cell bodies more clearly through visual inspection at higher
306 magnifications compared with lower magnifications, confirming that most neurons
307 identified at lower magnification were indeed NTS neuron cell bodies, which exhibited
308 clear responses to VNS.
309 Note that there was variability in VNS responsiveness among neurons detected within
310 the NTS (Figure 2D and E), prompting us to further examine their characteristics more
311 thoroughly by varying the stimulus conditions.
312
313
314 Diverse neuronal responses to VNS in the NTS
315 In vivo brainstem imaging was performed during VNS administered at various
316 intensities and frequencies to explore how NTS neurons respond to different intensities
317 and frequencies. Additionally, we assessed the responsiveness of the NTS neurons to
318 repetitive stimulation across different intensities and frequencies.
319 First, we set the stimulus frequency at 10 Hz and varied the stimulus intensities
320 (Figure 3A–E and Figures S4A, S5). Most of the stimulus-responsive NTS neurons

321 exhibited enhanced responses to higher stimulus intensities. On the other hand, one
322 neuron detected outside of the NTS showed only a spontaneous activity change and no
323 clear response to VNS (neuron #2 in Figure 3 and Figures S4, S5). NTS neurons showed
324 minimal responses to VNS at 0.1 mA and 0.25 mA and there was no clear difference
325 between these intensities, while there was a substantial increase in the neural response at
326 0.5 mA. The difference between 0.5 mA and lower intensities suggests a possible
327 threshold between them for recorded NTS neurons. At 1.0 mA, the responses increased
328 further. We also calculated various parameters for evaluating the neural responses and
329 observed consistent tendencies (Figure 3E).

330 We next evaluated the effect of repetitive stimulation on the neural responses at
331 various stimulus intensities (Figure 3C–D and Figure S4A). At 0.1 mA and 0.25 mA, we
332 did not observe a change in the responses to repeated stimulation at each stimulus
333 intensity. On the other hand, at higher intensities of 0.5 mA and 1.0 mA, with repeated
334 stimulations at 50-s intervals, some neurons exhibited gradually enhanced responses
335 during the session.

336 Next, using the same recorded neurons, we set the stimulus intensity at 1.0 mA and
337 varied the stimulus frequencies (Figure 3F–H and Figure S4B). The neuronal responses
338 to VNS increased gradually as the stimulus frequency was increased from 1 Hz to 10 Hz,
339 similar to when the stimulus intensity was increased. Interestingly, increasing the
340 frequency to 15 Hz resulted in a reduction in the neural response compared with that at
341 10 Hz. We also investigated the effects of repetitive stimulation during each session at
342 various frequencies. At 1 Hz, 2.5 Hz, and 5 Hz, we did not observe clear changes in
343 response to repeated stimulation during each session. At 10 Hz, however, most of the
344 NTS neurons showed a gradually increased response. Notably, at a higher frequency of
345 15 Hz, despite similar initial responses to those at 10 Hz, neurons exhibited decreased
346 responses to subsequent stimuli during the session.

347 These results indicate that repeated stimulation may uniquely affect synaptic
348 interactions and signal transmission between the vagus afferent nerve and NTS neurons.
349 While we consider the physiological mechanisms behind the observed acceleration and
350 deceleration below in the discussion section, our findings also suggest that the frequency-
351 dependent increase and decrease in responses to VNS are not merely artifacts caused by
352 the slow off-kinetics of GCaMP. Changes in neural activities and associated calcium

353 concentrations occur more rapidly than the signal changes detected by calcium indicators
354 like GCaMP. This discrepancy can theoretically lead to an artificial amplification of
355 baseline signals during repetitive stimuli, which may account for the increase in
356 fluorescent signals at 10Hz. Our imaging system, however, reliably detected an opposing
357 decrease in the GCaMP signal in response to repetitive stimulation at 15 Hz, despite
358 similar initial response levels to those observed at 10 Hz. Thus, the enhanced responses
359 at 10Hz are also likely to reflect the actual responses of the neurons, rather than being
360 artifacts.

361 Together, these findings indicate that the D-PSCAN method effectively detects
362 various types of neurons in the NTS under different stimulus conditions. This method
363 demonstrated that specific VNS conditions can directly and effectively modulate NTS
364 neuron activities, potentially influencing whole-brain neural networks involved in the
365 regulation of emotion.

366

367 Chemical stimulation triggered both immediate and long-lasting responses in NTS
368 neurons

369 Up to this point, we examined the response of NTS neurons to artificial electrical
370 stimulation of the vagus afferent nerve. Emotional responses are also governed by more
371 physiologic stimuli and conditions. To assess the suitability of the D-PSCAN method for
372 capturing responses under physiological conditions, we measured the activity of NTS
373 neurons following intravenous administration of CCK (Figure 4A). CCK is a hormone
374 released from the gastrointestinal tract before and after meals that directly influences the
375 afferent fibers of the vagus nerve and is proposed to transmit signals to various brain
376 regions, such as a feeding center[46], via the NTS. Also, to assess whether the intravenous
377 administration process itself affects neural activity, we monitored responses during saline
378 administration as a negative control. The timing of the intravenous administration was
379 determined by including SR101 in the injected solution and observing the signal detected
380 in the blood vessels surrounding the NTS using in vivo two-photon microscopy
381 (Supplementary Movie 3).

382 With this method, we first demonstrated that saline administration did not induce a
383 clear change in neural activity (Figure 4B–C and Supplementary Movie 4). In contrast,
384 CCK administration induced a change in NTS neuron activities (Figure 4B–C and

385 Supplementary Movie 5); upon administering CCK, we immediately observed clear and
386 significant signal changes in NTS neurons (Figure 4B–E). Additionally, more than 5
387 minutes after CCK administration, we observed a higher frequency of spontaneous
388 activity compared with before CCK administration or after saline administration (Figure
389 4C and Figure S6). These results demonstrate that the D-PSCAN method is applicable to
390 the detection of changes in NTS neuron activity induced under physiological conditions.
391

392 **Discussion:**

393 In the present study, to understand how the information processing mechanisms of
394 brain-viscera pathways mediated by the NTS regulate emotions, we developed a new
395 imaging technique named D-PSCAN based on in vivo two-photon imaging and double
396 prism-based optical access. This method enables wide-field observation of deep-brain
397 areas in the brainstem, including the NTS, while keeping the cerebellum, an important
398 region for emotional regulation, intact. We confirmed that the D-PSCAN method allows
399 for specific identification of NTS neurons, distinguishing them from surrounding regions
400 based on horizontal coordinates in its wide field of view. Additionally, based on the
401 advantages of two-photon imaging, we confirmed that the obtained signals originated
402 from the surface brainstem area, i.e., the NTS, rather than deeper regions such as 10N.
403 As we observed no GCaMP expression in 10N, it appears unlikely that vagal afferent
404 terminals were labeled by GCaMP, ensuring almost no or undetectable contamination of
405 their signal in the observed NTS areas. These findings together indicate that our method
406 provides specific identification of NTS activities and assesses their responsiveness to
407 VNS and CCK.

408 Using this method, we observed the responses of mouse NTS neurons to VNS, a
409 technique clinically employed to treat neuropsychiatric disorders in humans. We
410 confirmed that responses to electrical stimulation depended on the intensity and
411 frequency, observed a threshold-like effect, and found that repeated excessive stimulation
412 could reduce the responses. In addition to responses to artificial stimuli like VNS, we
413 detected significant immediate responses and smaller but sustained activities following
414 physiological stimuli such as CCK. These results demonstrate the usefulness of the D-
415 PSCAN method for investigating how the NTS neurons process information from visceral
416 organs for emotional regulation.

417 Recent studies have advanced our understanding of the complex mechanisms by
418 which the NTS processes various types of visceral information[24,35,38,47,48]. How these
419 mechanisms underlie the therapeutic effects of VNS and regulate emotion, however,
420 remains unclear. Our imaging technique, which allows for detailed observation of NTS
421 neuron activities while maintaining the integrity of cerebellar circuits crucial for
422 emotional regulation, is expected to be instrumental in deepening our knowledge of these
423 complex mechanisms.
424 Repeated VNS induced both enhanced and diminished NTS responses, depending on
425 the stimulus conditions. As discussed above, the observed NTS responses are unlikely to
426 be artifacts caused by the calcium indicator (GCaMP). These results indicate that repeated
427 stimulation may uniquely affect synaptic interactions and signal transmission between
428 the vagus afferent nerve and NTS neurons. Inhibitory interneurons in the NTS are also
429 involved in information processing during mechanical stimulation of digestive organs[35],
430 suggesting the possible contribution of such complex circuitries within the NTS for
431 adjusting the VNS signal. While an anodal block is likely to enhance specificity in
432 targeting vagal afferent fibers, VNS might also weakly stimulate efferent fibers, which in
433 turn might stimulate visceral organs and further activate the vagal afferent fibers. This
434 may also influence the rates of the neuron responses. Overall, as optimizing VNS
435 parameters for human patients is critical[13,49,50], our NTS imaging method in mice could
436 help reveal the underlying mechanisms of VNS, leading to more effective and
437 personalized therapy settings.
438 CCK may induce prolonged activation of the vagus afferent nerve[51,52]. The observed
439 spontaneous fluctuations in the GCaMP signal lasting for more than 5 minutes suggested
440 that CCK administration first induced prolonged activation of the vagus nerve, which
441 then indirectly activated the NTS. This finding demonstrates that the D-PSCAN method
442 has significant potential to detect changes in NTS neuron activity under physiological
443 conditions.
444 Overall, our development of the wide-field and deep-brain two-photon imaging
445 method utilizing a prism-based optical interface marks a significant advancement in the
446 ability to study the NTS in vivo while maintaining an intact cerebellum. Future
447 applications of this imaging system, particularly in awake animals, will be crucial for
448 understanding the dynamic interactions within the NTS and its role in neuropsychiatric
449 disorders. By enabling detailed observation of NTS activities, this method offers a

powerful tool for advancing our understanding of the vagus nerve's impact on brain function and emotional health, potentially leading to improved clinical interventions for neuropsychiatric conditions.

Funding

This study was supported by the JSPS KAKENHI Grant (grant number JP18K06536, JP20H05076, JP21H02801, JP22H05081, JP22H05519, JP24H01260 to M.A.), the Cooperative Study Program of National Institute for Physiological Sciences (19-233, 20-140 to M.S.; 21-244, 22NIPS218 to D.Y.), the practical research project for rare/intractable diseases from Agency for Medical Research and Development (AMED; Grant #: 20ek0109315h003 to M.S.), and the Research Grant for Neurological and Psychiatric Disorders from National Center of Neurology and Psychiatry, Japan (NCNP; Grant #: 30-3, 1-1, and 2-6 to M.S.).

Acknowledgements

We thank Okito Hashimoto for technical advice and discussion. We also thank the members of the laboratory for their help, especially Ikuko Takeda, Yuki Ichihashi, Ryo Fujikawa, and Fumiko Kito for experiments and data analyses.

Author Contributions

M.A., D.Y. and M.S. conceived and coordinated the whole project. M.A. designed and developed a method for double-prism-based *in vivo* two photon imaging with the support of T.K. and J.N.; M.A., D.Y., H.K., E.T. and M.S. performed imaging experiments during the VNS and CCK-administration; M.A., A.H., D.Y., and S.T. performed data analyses with the support of C.I., A.N., H.Y., A.S. and M.S.; M.A., A.H., D.Y., A.N., Y.A., and M.S. wrote the paper, with contributions from all authors.

Data availability

The data that support the findings of this study are available from the corresponding author upon reasonable request. The anatomical information in the Allen Brain Atlas (https://atlas.brain-map.org/) was used for the anatomical description, determination of the virus injection area, and evaluation of the recorded brain regions.

483

484 **Methods**

485

486 **Animals**. All animal experiments were carried out in accordance with National Institutes
487 of Health guidelines and approved by the National Institute for Physiological Sciences
488 Animal Care and Use Committee (approval number 18A102), or in accordance with the
489 National Institute of Neuroscience, National Center of Neurology and Psychiatry (Tokyo,
490 Japan) and were approved by the Institutional Animal Investigation Committee (approval
491 number: 2020004). Male C57BL/6 mice housed under a 12-h light/dark cycle with free
492 access to food and water were used for all experiments. Mice at 3–10 months of age were
493 used for the experiments.

494

495 **Virus injection**. Nucleus tractus solitarii (NTS) is a structure distributing in the dorsal
496 medulla near the area postrema. To express GCaMP, a genetically encoded calcium
497 indicator for monitoring neural activity, we used a gene expression system based on the
498 AAV vector. We tested AAV1/Syn.GCaMP6s, AAV1/Syn.GCaMP6f, and
499 AAVdj/Syn.GCaMP7f, which were produced as described previously[53,54] using plasmids
500 obtained from Addgene. As the GCaMP was expressed under the regulation of the Syn
501 (Synapsin) promoter, all of the recording targets were assumed to be neuron-specific. All
502 of the viruses allowed us to visualize the neural activity in the NTS, and type of virus
503 used in each experiment is indicated in each corresponding figure legend. Viruses were
504 injected into mice at approximately postnatal day (P) 50–60 for experiments at least 1
505 month before the microprism implantation, which was followed by *in vivo* imaging.
506 Injection procedures were performed as described previously[55], with some modifications
507 to target the NTS efficiently. During surgery, the mice were anesthetized with isoflurane
508 (initially 2% [partial pressure in air] and then reduced to 1%). A small circle (~1 mm in
509 diameter) of the skull was thinned over the cerebellum (around the injection site) using a
510 dental drill to mark the site for a small craniotomy. Viruses were injected into the bilateral
511 NTS regions at two sites (depth 4.7 and 3.7 mm from the dorsal surface of the cerebellum,
512 volume 250 nl/site, at 100 nl/min) to sufficiently cover the NTS, over a 5-min period at
513 each depth using a UMP3 microsyringe pump (World Precision Instruments). The X-Y
514 coordinates for the injection site were usually 0.5 mm lateral to the midline and 3.3 mm
515 caudal to lambda. The beveled side of the injection needle was faced to the caudal so that

516 the needle could be smoothly inserted into and passed through the cerebellum, and the
517 AAV would cover the NTS similarly in both hemispheres. We designed our injection
518 protocol (especially the volume and depth) carefully to widely cover the area around the
519 NTS, while the anatomical coordinates of the field of view for the two-photon imaging
520 were precisely targeted using visual guide through the microprism implanted as described
521 below (see the section "In vivo two-photon imaging in the wide brainstem area"). Also,
522 as shown in Figure 1B, the expression of GCaMP was excluded in the 10N area, which
523 placed next to and ventrally to the NTS as marked by the ChAT immunostaining. The
524 reason for the exclusion is unclear, but it may be because the promoters and/or serotypes
525 used in the present studies do not match for inducing the GCaMP expression in these
526 ChAT-positive neurons. In any case, since neurons in the 10N area receive synaptic inputs
527 from NTS neurons[6,56] and are a source of vagal efferents, the lack of expression in the
528 neurons of this area rather positively aids in the interpretation of the GCaMP signals
529 detected by in vivo NTS imaging. In some mice, a deeper area (more than 0.5 mm from
530 the dorsal surface of the brainstem, i.e., the surface of the microprism) also expressed the
531 GCaMP when the fluorescence was checked in the brain slices (Figure 1B), but this
532 deeper area was beyond the deepest limit of our two-photon imaging system for the
533 detection of the sufficient signal intensity through the double prism *in vivo*. These results
534 indicates that our recording system simply allows specific targeting of the neurons within
535 the NTS and together with laterally-surrounding wide areas.
536
537 **In vivo two-photon imaging in the wide brainstem area**. We developed a novel,
538 minimally invasive method based on the double prism, which allows in vivo two-photon
539 imaging of deep brain regions, specifically around the NTS. This innovative approach
540 also enables simultaneous vagus nerve stimulation (VNS) or intravenous administration
541 of cholecystokinin-8 (CCK).
542 In vivo two-photon imaging was performed as described previously[55,57], with some
543 special development for the optical access to the brainstem and NTS as explained below.
544 Before the surgery, we designed an implantable double microprism assembly, comprising
545 a 2-mm right-angle glass microprism (TS N-BK7, 2 mm AL+MgF2, Edmund) bonded to
546 another 2-mm right-angle glass microprism and a 3 x 3, 3 × 4 or 4 × 4 mm cover glass
547 window (No.1; Matsunami) at the surface-end position of the imaging window, was
548 prepared. Dental cement was used to fix this assembly at the correct position for NTS

549 imaging. The cover glass was used to enhance adhesion to the dental cement, securing
550 the position of the double microprism assembly and preventing dental cement from
551 obstructing its optical path. We implanted the assembly (or simply termed 'double prism')
552 between the cerebellum and the brainstem using a custom-made vacuum-based
553 manipulator (Figure 1D and Figures S1A–B).
554 At 1–8 months after the virus injection, the mice were anesthetized with isoflurane
555 (initially 2% [partial pressure in air] and reduced to 1% during the surgery). For the
556 implantation of the double prism, the skull over the dorsal surface of the cerebellum was
557 carefully removed using a dental drill and fine forceps (Figure S1C–D). A micro-knife
558 was used to incise the thick dura mater between the posterior edge of the cerebellum and
559 the spinal cord. Removing the dura mater over the cerebellum not only allows for smooth
560 insertion of the prism but also adequately relieves the pressure that might occur when the
561 prism is inserted between the cerebellum and the brainstem.
562 Next, the newly developed vacuum-based prism holder was used to insert and implant
563 the double prism between the cerebellum and the brainstem (Figure 1D–E, Figure S1A–
564 B, E). Sufficient space and no neural fibers remained between the cerebellum and the
565 brainstem around the NTS area, enabling smooth insertion of the prism without cutting
566 neural fibers. Using a stereotaxic frame and vacuum-based prism holder attached to an
567 equipped manipulator, the prism can be precisely operated during the implantation while
568 being maintained in a horizontal position. The vacuum-based prism holder has a hook on
569 one side (Figure 1D and Figure S1A–B), which exerts a pushing force when sliding the
570 sharp corner of the double prism between the cerebellum and the brainstem from the
571 caudal side to the rostral side (Figure 1D–E). After slowly inserting the double prism to
572 approximately 1.6 mm deep, we waited a few minutes to ensure that breathing and other
573 physical conditions were not disturbed (Figure 1E). The double prism was slid further
574 down at 0.1-mm increments until reaching a maximum depth of 2.0 mm. Any physical
575 reactions such as disrupted breathing occurring during the insertion led us to promptly
576 retract the prism. When retracting the double prism assembly, it is crucial to ensure that
577 the suction force by the vacuum is sufficient, as insufficient suction may lead to failure
578 of the retraction. The area directly beneath the microprism was minimally compressed
579 but remained intact, minimizing motion artifacts caused by the animal's breathing. Setting
580 a stereomicroscope at an angle such that the brainstem can be visualized through the

581 double prism allows for clear observation of the arrangement of blood vessels in the
582 brainstem and fourth ventricle while inserting the prism. Bleeding was rarely observed
583 during the implantation procedure.

584 After the double prism was fully inserted, UV craft resin was used to fix the double
585 prism and coat the surface of the targeted nerve structures (Figure S1F), followed by tight
586 fixation with dental cement. A resin coating was applied with the double prism remaining
587 in the holder and maintaining sufficient contact with the brainstem target area (including
588 the NTS) to prevent the resin from getting between them. After the UV resin had cured,
589 the holder was carefully released, and the double prism was firmly fixed to the
590 surrounding areas, including the remaining skull bone rostral to the cerebellum, using
591 dental cement. For the further head fixation for two-photon imaging under the microscope
592 objective, the head plate was attached to the skull with dental cement (Figure 1F).

593 The double prism allows for optical access to the brainstem located on the ventral side
594 of the cerebellum, which exceeds 2.0 mm in thickness. Using the wide field of view and
595 horizontal coordinates, the position of the fourth ventricle serves as a key reference for
596 locating the NTS. Two-photon imaging through the double prism enabled us to detect
597 neural activities in the NTS at the single-cell resolution, visualized by GCaMP (Figure
598 1G). We named this method 'D-PSCAN', or Double-Prism based brainStem imaging
599 under Cerebellar Architecture and Neural circuits.

600 During the consecutive imaging sessions, mice were anesthetized with isoflurane
601 (1%) or a ketamine (70 mg/kg) and xylazine (10.5 mg/kg) mixture (see the sections below
602 for more details). Experiments were performed in a completely dark environment. The
603 activity of NTS neurons was recorded by imaging fluorescence changes with a
604 multiphoton microscope (Nikon A1R MP, Nikon) and a Mai Tai DeepSee Ti:sapphire
605 laser (Spectra-Physics) at 920 nm, through a 4x dry objective, 0.28 N.A. (Olympus).
606 Scanning and image acquisition were controlled by NIS-elements software (Nikon).
607 Brain motion artifacts interfered with imaging in awake mice but were minimized under
608 anesthesia, enabling the stable detection of the neural activities at a single cellular
609 resolution both in and out of the NTS area (Figure 2, Figure S3 and Supplementary Movie
610 1 and 2). Time-lapse imaging at various depths was performed by adjusting the imaging
611 focal plane using a piezo to move up and down in depth (Figure 2A and Figure S3).
612 Volumetric live imaging (2 mm x 2 mm horizontally, or smaller for zooming, 200–480

613 μm dorsoventrally, at around 0.4–1.0 Hz temporal resolution) of neural activities in the
614 wide brainstem area (including the NTS) of the head-fixed mouse was performed through
615 the implanted double prism. Importantly, this wide field of view and piezo-based
616 volumetric imaging allowed us to detect the GCaMP fluorescence and neural activities
617 not only from inside but also from outside of the NTS areas and confirm the specificity
618 of the stimulus-evoked responses in the NTS, as explained below.
619
620 **Vagus nerve stimulation during NTS imaging.** For the NTS imaging experiments with
621 vagus nerve stimulation (VNS), a bipolar platinum hook electrode, connected to a
622 programmable stimulator (SEN-8203, NIHON KODEN, Tokyo, Japan) and isolator (SS-
623 202J, NIHON KODEN), was wrapped around the cervical vagal trunk, and was fixed and
624 insulated from surrounding tissue using the quick-setting silicone adhesive Kwick-Sil™
625 (World Precision Instruments, FL, USA). Then, the mouse's head was fixed under the
626 objective lens by using the head plate tightly attached to the skull under anesthesia (a
627 ketamine [70 mg/kg] and xylazine [10.5 mg/kg] mixture). VNS was triggered using
628 custom Labview software. To determine optimal stimulation parameters VNS was
629 delivered in blocked trials for 10 s at the frequencies of 1.0, 2.5, 5.0, 10, or 15 Hz, at the
630 intensities of 0.1, 0.25, 0.5, or 1.0 mA, with a pulse width of 100 μs. The maximum
631 current intensity and frequency of stimulation were set at 1.0 mA and 10 Hz according to
632 the previous study[39,44]. The first VNS train was delivered at least 10 s after the start of
633 imaging, and VNS was repeated three times in total (Figure 3 and Figures S4, S5), or
634 more (Figure 2), with a 50-s interval. Neither facial nor muscle twitching (an indication
635 of off-target stimulation of musculature surrounding the vagus nerve) was observed with
636 any parameters used in any of the mice included in the present study. VNS and NTS
637 imaging were performed with the mouse head fixed under the microscope objective lens
638 using the head plate. The timings of the imaging and VNS were synchronously recorded
639 with image acquisition (GCaMP imaging in NTS) using NI software (Labview; National
640 Instruments) and NI-DAQ (National Instruments).
641
642 **Intravenous administration of CCK during NTS imaging.** To examine the neural
643 activity change in response to more physiological stimulation than VNS, we employed
644 cholecystokinin octapeptide (CCK); it has been demonstrated that intravenous

645 administration of CCK activates vagal afferents and increases firing rate of hepatic branch
646 of the vagus nerve[52] (Cox and Randich, 1997). On the day of the experiment, mouse's
647 head was fixed under the objective lens by using the head plate tightly attached to the
648 skull under anesthesia (1% isoflurane). During the Ca^{2+} imaging, CCK solution (2.0
649 μg/kg) or saline was mixed with sulforhodamine 101 (SR101; 0.1 mM) and intravenously
650 administered through the tail vein. 60 s after the start of the imaging, saline with SR101
651 was intravenously administered and performed for 10 minutes. Using the same animal,
652 60 s after the beginning of the imaging, CCK with SR101 was intravenously administered
653 and performed for 15 minutes. Intravenous administration and NTS imaging were
654 performed with the mouse head fixed under the microscope objective lens using the head
655 plate.
656
657 **Imaging data analyses and statistics.**
658 The activity of NTS neurons was recorded by imaging fluorescence changes with a
659 multiphoton microscope (Nikon A1R MP, Nikon). Time-lapse imaging at various depths
660 was performed by adjusting the imaging focal plane using a piezo to move up and down
661 in depth (Figure 2A and Figure S3). The volumetric live imaging (at around 0.4–1.0 Hz
662 temporal resolution) of NTS neural activities was performed through the implanted
663 double prism. We recorded a total of 10–16 focal planes (z-planes) at each time point for
664 each mouse. In an example case (Figure 2D), we recorded a total of 16 z-planes at each
665 time point. We stacked every 4 consecutive plane from top to bottom to create an average
666 image for each time point. This stacking was done with a two-plane overlap; for instance,
667 the first stack included the 1st to 4th z-planes, the second stack included the 3rd to 6th z-
668 planes, and subsequent stacks followed this pattern. As a result, we obtained 7 stacked
669 planes in total in this experiment, labeled as Zp1 through Zp7, respectively. This
670 procedure is advantageous to enhance the signal to noise ratio in each movie, which is
671 critical for further automatic detection of the active neurons[45]. After the automatic
672 detection of the active neurons, we checked the existence of the overlapped detection of
673 the regions of interest (ROIs, i.e., active neurons) between adjacent Zps next each other,
674 and removed such overlaps by the manual inspection.
675 Importantly, before stacking 4 consecutive z-planes at each time point as explained
676 above, they were processed to correct for brain motion artifacts using the enhanced
677 correlation coefficient image alignment algorithm[58]. For this z-axis correction, first (most

678 dorsal surface frame) was used as a reference for correcting the second z-plane. Then, an
679 average image of these two aligned z-planes was further used for the correction of the
680 third z-plane. Eventually an average image of these three aligned z-planes was used for
681 the motion correction of the fourth z-plane. Through this procedure, four z-planes were
682 motion corrected and used to accurately obtain a stacked (averaged) image for each Zp at
683 each time point. Next, the time-series of stacked GCaMP images at each Zp was further
684 processed to correct for brain motion artifacts using the enhanced correlation coefficient
685 image alignment algorithm[58]. Temporal dynamics of neural activity were clearly observed
686 at multiple depths after this motion correction procedure (Supplementary Movie 1 and 2).
687 These motion-corrected movies were used for automatic ROI detection. The ROIs for
688 the detection of neural activity were automatically selected using a constrained
689 nonnegative matrix factorization algorithm in MATLAB R2014a/R2019b as described
690 previously[45,57], with some manual adjustments as described above. The same constrained
691 nonnegative matrix factorization package for ROI detection also provides an option for
692 signal processing and measurement of the signal change (ΔF/F) of each neuron. We used
693 this method to identify neurons and calculate ΔF/F for them. While neurons for the
694 analyses were initially automatically detected, neurons responding to noisy signals with
695 no apparent calcium transient at any time during the experimental days were identified
696 by visual inspection and excluded from further analysis. To apply the same regions of
697 interest (ROIs) for analyzing images obtained across multiple conditions (i.e., various
698 VNS conditions or saline vs CCK experiments), the movies from the same mouse and the
699 same field of view were precisely aligned with each other using the same enhanced
700 correlation coefficient algorithm as above, and these multiple movies of the same field of
701 view were tentatively concatenated for the ΔF/F measurement. The obtained ΔF/F data
702 were eventually separated to evaluate the neural responses under each condition.
703 For the statistical analysis, we used MATLAB R2022a/R2023b. The Wilcoxon
704 signed-rank tests for paired comparisons was used to determine statistical significance
705 ($p < 0.05$) in Figure 4. Two-tailed tests were selected for all statistical analyses. Graphs
706 were produced by MATLAB R2022a/R2023b.
707 As for the imaging data analysis, one concern was that the off kinetics of the GcaMP6f
708 signal might not be sufficiently fast to consider the responses to 3 trails of VNS as
709 independent data, and thus statistical evaluation based on these responses might not be
710 reliable to evaluate the neural responses. As shown in Fig. 3G, however, neurons showed

711 a reduced response to repeated stimulation, indicating that calcium signaling was not
712 enhanced by delayed off-kinetics.
713
714 **Drugs**
715 CCK was purchased from PEPTIDE INSTITUTE, INC. (Osaka, Japan) and was
716 dissolved in saline (2.0 μg/kg). In addition, sulforhodamine (SR101), a red fluorescent
717 dye, is diluted to 0.1 mM in saline or CCK solution to confirm the successful intravenous
718 administration and the injection timing during NTS imaging.
719
720 **References**

721 1. Khalsa, S.S., Adolphs, R., Cameron, O.G., Critchley, H.D., Davenport, P.W.,
722 Feinstein, J.S., Feusner, J.D., Garfinkel, S.N., Lane, R.D., Mehling, W.E., et al.
723 (2018). Interoception and Mental Health: A Roadmap. Biol Psychiatry Cogn
724 Neurosci Neuroimaging *3*, 501-513. 10.1016/j.bpsc.2017.12.004.
725 2. Chen, W.G., Schloesser, D., Arensdorf, A.M., Simmons, J.M., Cui, C.,
726 Valentino, R., Gnadt, J.W., Nielsen, L., Hillaire-Clarke, C.S., Spruance, V., et al.
727 (2021). The Emerging Science of Interoception: Sensing, Integrating,
728 Interpreting, and Regulating Signals within the Self. Trends Neurosci *44*, 3-16.
729 10.1016/j.tins.2020.10.007.
730 3. Dantzer, R., O'Connor, J.C., Freund, G.G., Johnson, R.W., and Kelley, K.W.
731 (2008). From inflammation to sickness and depression: when the immune
732 system subjugates the brain. Nat Rev Neurosci *9*, 46-56. 10.1038/nrn2297.
733 4. Yamada, T., and Katagiri, H. (2007). Avenues of communication between the
734 brain and tissues/organs involved in energy homeostasis. Endocr J *54*, 497-505.
735 10.1507/endocrj.kr-106.
736 5. D'Mello, C., and Swain, M.G. (2011). Liver-brain inflammation axis. Am J
737 Physiol Gastrointest Liver Physiol *301*, G749-761. 10.1152/ajpgi.00184.2011.
738 6. Berthoud, H.R., and Neuhuber, W.L. (2000). Functional and chemical anatomy
739 of the afferent vagal system. Auton Neurosci *85*, 1-17. 10.1016/S1566-
740 0702(00)00215-0.

7. Beekwilder, J.P., and Beems, T. (2010). Overview of the clinical applications of vagus nerve stimulation. J Clin Neurophysiol *27*, 130-138. 10.1097/WNP.0b013e3181d64d8a.

8. Bonaz, B., Picq, C., Sinniger, V., Mayol, J.F., and Clarencon, D. (2013). Vagus nerve stimulation: from epilepsy to the cholinergic anti-inflammatory pathway. Neurogastroenterol Motil *25*, 208-221. 10.1111/nmo.12076.

9. Penry, J.K., and Dean, J.C. (1990). Prevention of intractable partial seizures by intermittent vagal stimulation in humans: preliminary results. Epilepsia *31 Suppl 2*, S40-43. 10.1111/j.1528-1157.1990.tb05848.x.

10. Groves, D.A., and Brown, V.J. (2005). Vagal nerve stimulation: a review of its applications and potential mechanisms that mediate its clinical effects. Neurosci Biobehav Rev *29*, 493-500. 10.1016/j.neubiorev.2005.01.004.

11. Wang, Y., Zhan, G., Cai, Z., Jiao, B., Zhao, Y., Li, S., and Luo, A. (2021). Vagus nerve stimulation in brain diseases: Therapeutic applications and biological mechanisms. Neurosci Biobehav Rev *127*, 37-53. 10.1016/j.neubiorev.2021.04.018.

12. Thompson, S.L., O'Leary, G.H., Austelle, C.W., Gruber, E., Kahn, A.T., Manett, A.J., Short, B., and Badran, B.W. (2021). A Review of Parameter Settings for Invasive and Non-invasive Vagus Nerve Stimulation (VNS) Applied in Neurological and Psychiatric Disorders. Front Neurosci *15*, 709436. 10.3389/fnins.2021.709436.

13. Heck, C., Helmers, S.L., and DeGiorgio, C.M. (2002). Vagus nerve stimulation therapy, epilepsy, and device parameters: scientific basis and recommendations for use. Neurology *59*, S31-37. 10.1212/wnl.59.6_suppl_4.s31.

14. Krahl, S.E., Clark, K.B., Smith, D.C., and Browning, R.A. (1998). Locus coeruleus lesions suppress the seizure-attenuating effects of vagus nerve stimulation. Epilepsia *39*, 709-714. 10.1111/j.1528-1157.1998.tb01155.x.

15. Krahl, S.E., Senanayake, S.S., and Handforth, A. (2001). Destruction of peripheral C-fibers does not alter subsequent vagus nerve stimulation-induced seizure suppression in rats. Epilepsia *42*, 586-589. 10.1046/j.1528-1157.2001.09700.x.

16. Jiang, Y., Li, L., Liu, B., Zhang, Y., Chen, Q., and Li, C. (2014). Vagus nerve stimulation attenuates cerebral ischemia and reperfusion injury via endogenous

774 cholinergic pathway in rat. PLoS One *9*, e102342.
775 10.1371/journal.pone.0102342.
776 17. Shao, P., Li, H., Jiang, J., Guan, Y., Chen, X., and Wang, Y. (2023). Role of
777 Vagus Nerve Stimulation in the Treatment of Chronic Pain.
778 Neuroimmunomodulation *30*, 167-183. 10.1159/000531626.
779 18. Furmaga, H., Shah, A., and Frazer, A. (2011). Serotonergic and noradrenergic
780 pathways are required for the anxiolytic-like and antidepressant-like behavioral
781 effects of repeated vagal nerve stimulation in rats. Biol Psychiatry *70*, 937-945.
782 10.1016/j.biopsych.2011.07.020.
783 19. Krahl, S.E., Senanayake, S.S., Pekary, A.E., and Sattin, A. (2004). Vagus nerve
784 stimulation (VNS) is effective in a rat model of antidepressant action. J
785 Psychiatr Res *38*, 237-240. 10.1016/j.jpsychires.2003.11.005.
786 20. Noble, L.J., Souza, R.R., and McIntyre, C.K. (2019). Vagus nerve stimulation as
787 a tool for enhancing extinction in exposure-based therapies.
788 Psychopharmacology (Berl) *236*, 355-367. 10.1007/s00213-018-4994-5.
789 21. Reid, S.A. (1990). Surgical technique for implantation of the neurocybernetic
790 prosthesis. Epilepsia *31 Suppl 2*, S38-39. 10.1111/j.1528-1157.1990.tb05847.x.
791 22. Lu, K.H., Cao, J., Phillips, R., Powley, T.L., and Liu, Z. (2020). Acute effects of
792 vagus nerve stimulation parameters on gastric motility assessed with magnetic
793 resonance imaging. Neurogastroenterol Motil *32*, e13853. 10.1111/nmo.13853.
794 23. Ahmed, U., Chang, Y.C., Cracchiolo, M., Lopez, M.F., Tomaio, J.N., Datta-
795 Chaudhuri, T., Zanos, T.P., Rieth, L., Al-Abed, Y., and Zanos, S. (2020). Anodal
796 block permits directional vagus nerve stimulation. Sci Rep *10*, 9221.
797 10.1038/s41598-020-66332-y.
798 24. Paton, J.F. (1999). The Sharpey-Schafer prize lecture: nucleus tractus solitarii:
799 integrating structures. Exp Physiol *84*, 815-833.
800 25. Hornby, P.J. (2001). Receptors and transmission in the brain-gut axis. II.
801 Excitatory amino acid receptors in the brain-gut axis. Am J Physiol Gastrointest
802 Liver Physiol *280*, G1055-1060. 10.1152/ajpgi.2001.280.6.G1055.
803 26. Travagli, R.A., Hermann, G.E., Browning, K.N., and Rogers, R.C. (2006).
804 Brainstem circuits regulating gastric function. Annu Rev Physiol *68*, 279-305.
805 10.1146/annurev.physiol.68.040504.094635.

27. Zheng, H., Patterson, L.M., Morrison, C., Banfield, B.W., Randall, J.A., Browning, K.N., Travagli, R.A., and Berthoud, H.R. (2005). Melanin concentrating hormone innervation of caudal brainstem areas involved in gastrointestinal functions and energy balance. Neuroscience *135*, 611-625. 10.1016/j.neuroscience.2005.06.055.
28. Ritter, R.C. (2011). A tale of two endings: modulation of satiation by NMDA receptors on or near central and peripheral vagal afferent terminals. Physiol Behav *105*, 94-99. 10.1016/j.physbeh.2011.02.042.
29. Julio-Pieper, M., Flor, P.J., Dinan, T.G., and Cryan, J.F. (2011). Exciting times beyond the brain: metabotropic glutamate receptors in peripheral and non-neural tissues. Pharmacol Rev *63*, 35-58. 10.1124/pr.110.004036.
30. Kline, D.D. (2008). Plasticity in glutamatergic NTS neurotransmission. Respir Physiol Neurobiol *164*, 105-111. 10.1016/j.resp.2008.04.013.
31. Traub, R.J., Sengupta, J.N., and Gebhart, G.F. (1996). Differential c-fos expression in the nucleus of the solitary tract and spinal cord following noxious gastric distention in the rat. Neuroscience *74*, 873-884. 10.1016/0306-4522(96)00173-x.
32. Naritoku, D.K., Terry, W.J., and Helfert, R.H. (1995). Regional induction of fos immunoreactivity in the brain by anticonvulsant stimulation of the vagus nerve. Epilepsy Res *22*, 53-62. 10.1016/0920-1211(95)00035-9.
33. Chae, J.H., Nahas, Z., Lomarev, M., Denslow, S., Lorberbaum, J.P., Bohning, D.E., and George, M.S. (2003). A review of functional neuroimaging studies of vagus nerve stimulation (VNS). J Psychiatr Res *37*, 443-455. 10.1016/s0022-3956(03)00074-8.
34. Lomarev, M., Denslow, S., Nahas, Z., Chae, J.H., George, M.S., and Bohning, D.E. (2002). Vagus nerve stimulation (VNS) synchronized BOLD fMRI suggests that VNS in depressed adults has frequency/dose dependent effects. J Psychiatr Res *36*, 219-227. 10.1016/s0022-3956(02)00013-4.
35. Ran, C., Boettcher, J.C., Kaye, J.A., Gallori, C.E., and Liberles, S.D. (2022). A brainstem map for visceral sensations. Nature *609*, 320-326. 10.1038/s41586-022-05139-5.
36. Adamaszek, M., Manto, M., and Schutter, D.J.L.G. (2022). The Emotional Cerebellum https://doi.org/10.1007/978-3-030-99550-8.

37. Armstrong, D.M., Rotler, A., Hersh, L.B., and Pickel, V.M. (1988). Localization of choline acetyltransferase in perikarya and dendrites within the nuclei of the solitary tracts. J Neurosci Res *20*, 279-290. 10.1002/jnr.490200302.
38. Zhao, Q., Yu, C.D., Wang, R., Xu, Q.J., Dai Pra, R., Zhang, L., and Chang, R.B. (2022). A multidimensional coding architecture of the vagal interoceptive system. Nature *603*, 878-884. 10.1038/s41586-022-04515-5.
39. Caravaca, A.S., Gallina, A.L., Tarnawski, L., Tracey, K.J., Pavlov, V.A., Levine, Y.A., and Olofsson, P.S. (2019). An Effective Method for Acute Vagus Nerve Stimulation in Experimental Inflammation. Front Neurosci *13*, 877. 10.3389/fnins.2019.00877.
40. Vuckovic, A., Tosato, M., and Struijk, J.J. (2008). A comparative study of three techniques for diameter selective fiber activation in the vagal nerve: anodal block, depolarizing prepulses and slowly rising pulses. J Neural Eng *5*, 275-286. 10.1088/1741-2560/5/3/002.
41. Brindley, G.S., and Craggs, M.D. (1980). A technique for anodally blocking large nerve fibres through chronically implanted electrodes. J Neurol Neurosurg Psychiatry *43*, 1083-1090. 10.1136/jnnp.43.12.1083.
42. Cunningham, J.T., Mifflin, S.W., Gould, G.G., and Frazer, A. (2008). Induction of c-Fos and DeltaFosB immunoreactivity in rat brain by Vagal nerve stimulation. Neuropsychopharmacology *33*, 1884-1895. 10.1038/sj.npp.1301570.
43. Yap, J.Y.Y., Keatch, C., Lambert, E., Woods, W., Stoddart, P.R., and Kameneva, T. (2020). Critical Review of Transcutaneous Vagus Nerve Stimulation: Challenges for Translation to Clinical Practice. Front Neurosci *14*, 284. 10.3389/fnins.2020.00284.
44. Cao, J., Lu, K.H., Powley, T.L., and Liu, Z. (2017). Vagal nerve stimulation triggers widespread responses and alters large-scale functional connectivity in the rat brain. PLoS One *12*, e0189518. 10.1371/journal.pone.0189518.
45. Pnevmatikakis, E.A., Soudry, D., Gao, Y., Machado, T.A., Merel, J., Pfau, D., Reardon, T., Mu, Y., Lacefield, C., Yang, W., et al. (2016). Simultaneous Denoising, Deconvolution, and Demixing of Calcium Imaging Data. Neuron *89*, 285-299. 10.1016/j.neuron.2015.11.037.

871 46. Rogers, R.C., and Hermann, G.E. (2008). Mechanisms of action of CCK to
872 activate central vagal afferent terminals. Peptides *29*, 1716-1725.
873 10.1016/j.peptides.2008.06.023.
874 47. Altschuler, S.M., Bao, X.M., Bieger, D., Hopkins, D.A., and Miselis, R.R.
875 (1989). Viscerotopic representation of the upper alimentary tract in the rat:
876 sensory ganglia and nuclei of the solitary and spinal trigeminal tracts. J Comp
877 Neurol *283*, 248-268. 10.1002/cne.902830207.
878 48. Chen, C.H., Williams, J.L., and Lutherer, L.O. (1994). Cerebellar lesions alter
879 autonomic responses to transient isovolaemic changes in arterial pressure in
880 anaesthetized cats. Clin Auton Res *4*, 263-272. 10.1007/BF01827432.
881 49. Souza, R.R., Robertson, N.M., McIntyre, C.K., Rennaker, R.L., Hays, S.A., and
882 Kilgard, M.P. (2021). Vagus nerve stimulation enhances fear extinction as an
883 inverted-U function of stimulation intensity. Exp Neurol *341*, 113718.
884 10.1016/j.expneurol.2021.113718.
885 50. Clark, K.B., Naritoku, D.K., Smith, D.C., Browning, R.A., and Jensen, R.A.
886 (1999). Enhanced recognition memory following vagus nerve stimulation in
887 human subjects. Nat Neurosci *2*, 94-98. 10.1038/4600.
888 51. Blackshaw, L.A., and Grundy, D. (1990). Effects of cholecystokinin (CCK-8) on
889 two classes of gastroduodenal vagal afferent fibre. J Auton Nerv Syst *31*, 191-
890 201. 10.1016/0165-1838(90)90185-l.
891 52. Cox, J.E., and Randich, A. (1997). CCK-8 activates hepatic vagal C-fiber
892 afferents. Brain Res *776*, 189-194. 10.1016/s0006-8993(97)01036-6.
893 53. Lock, M., Alvira, M., Vandenberghe, L.H., Samanta, A., Toelen, J., Debyser, Z.,
894 and Wilson, J.M. (2010). Rapid, simple, and versatile manufacturing of
895 recombinant adeno-associated viral vectors at scale. Hum Gene Ther *21*, 1259-
896 1271. 10.1089/hum.2010.055.
897 54. Shibata, A.C.E., Ueda, H.H., Eto, K., Onda, M., Sato, A., Ohba, T., Nabekura, J.,
898 and Murakoshi, H. (2021). Photoactivatable CaMKII induces synaptic plasticity
899 in single synapses. Nat Commun *12*, 751. 10.1038/s41467-021-21025-6.
900 55. Agetsuma, M., Hamm, J.P., Tao, K., Fujisawa, S., and Yuste, R. (2018).
901 Parvalbumin-Positive Interneurons Regulate Neuronal Ensembles in Visual
902 Cortex. Cereb Cortex *28*, 1831-1845. 10.1093/cercor/bhx169.

56. Davis, S.F., Derbenev, A.V., Williams, K.W., Glatzer, N.R., and Smith, B.N. (2004). Excitatory and inhibitory local circuit input to the rat dorsal motor nucleus of the vagus originating from the nucleus tractus solitarius. Brain Res *1017*, 208-217. 10.1016/j.brainres.2004.05.049.

57. Agetsuma, M., Sato, I., Tanaka, Y.R., Carrillo-Reid, L., Kasai, A., Noritake, A., Arai, Y., Yoshitomo, M., Inagaki, T., Yukawa, H., et al. (2023). Activity-dependent organization of prefrontal hub-networks for associative learning and signal transformation. Nat Commun *14*, 5996. 10.1038/s41467-023-41547-5.

58. Evangelidis, G.D., and Psarakis, E.Z. (2008). Parametric image alignment using enhanced correlation coefficient maximization. IEEE transactions on pattern analysis and machine intelligence *30*, 1858-1865. 10.1109/TPAMI.2008.113.

Figures (from next page)

Figure. 1

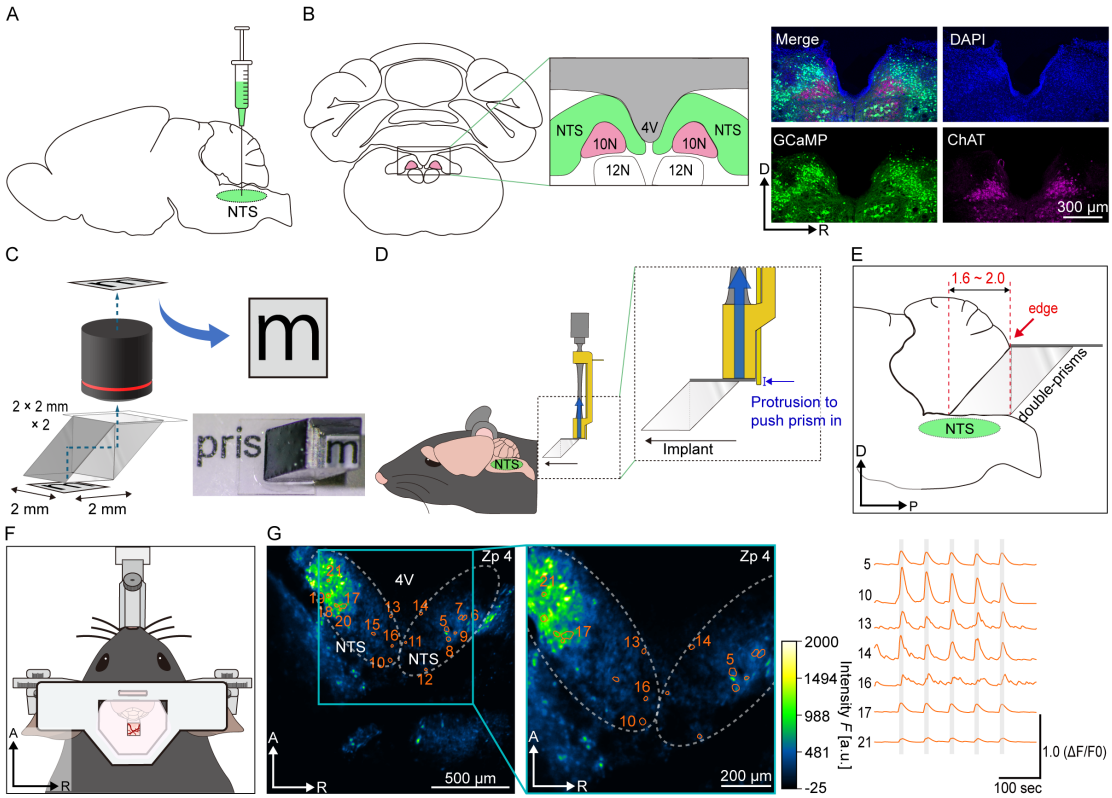

Figure 1. Schematic overview of in vivo NTS imaging with a double prism

(A) Sagittal view of a mouse brain illustrating how GCaMP was expressed in NTS neurons by AAV injection.

(B) GCaMP expression in the NTS. (left) Schematic illustration of the injection site modified from the Allen Brain Atlas. (right) Expression of GCaMP (green) in the NTS, exclusive to the 10N area (marked by ChAT immunohistochemical staining in magenta). Blue, DAPI.

(C) Two 2-mm right-angled prisms are attached to each other using UV-curable optical adhesive and bonded to a 3 × 3 mm square cover glass. In this illustration, the letter “m” in the word “prism” appears through the double prism.

(D) A vacuum-type prism holder is used to implant the double prism. Black arrows indicate the directions in which the double prisms are pushed forward. Red arrows indicate directions in which the double prisms are vacuumed up to be held by the holder.

(E) Implantation of the double prism. The double prism is carefully inserted between the cerebellum and the brainstem approximately 1.6−2.0 mm from the posterior edge of the cerebellum. The area containing the NTS is observed through the double prism.

934 (F) A head plate is attached to the mouse skull using dental cement after the microprism
935 implantation.
936 (G) Example of in vivo brainstem imaging showing neural activity in a live mouse. Left:
937 Representative two-photon imaging of GCaMP fluorescence in a large field of view covering
938 the wide brainstem area in response to VNS. Each number in the image indicates regions of
939 interest (ROIs), each corresponding to a putative single neuron. Median fluorescence over
940 time is presented in green-fire-blue to show a baseline fluorescence level. Middle: Magnified
941 view. Right: Representative traces showing changes in GCaMP signal over baseline ($\Delta F/F0$)
942 over time in each ROI. Gray indicates the timing of VNS. Zp4, 4th z-stacked plane obtained
943 by the volumetric scanning (see also Figure 2A and Figure S3).
944 D, dorsal; R, right; P, posterior; A, anterior.

Figure. 2

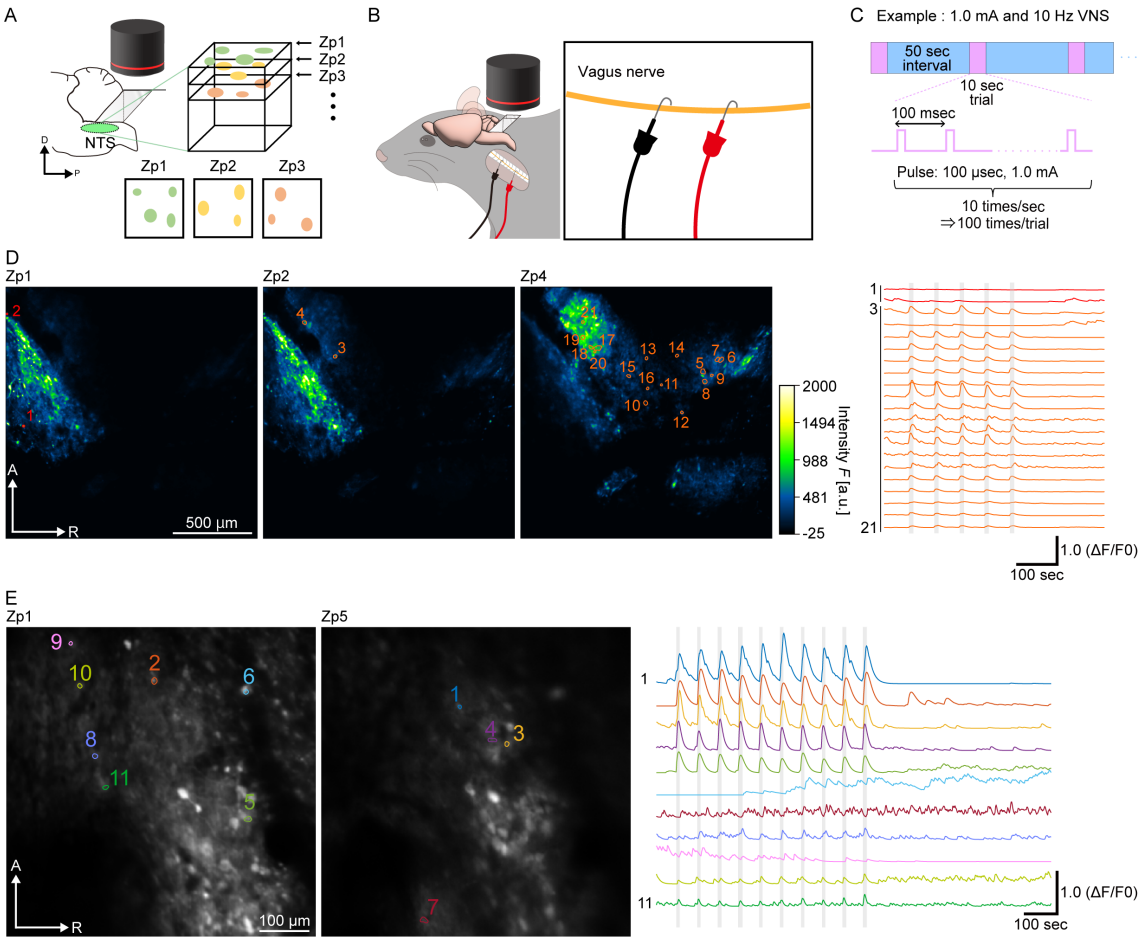

Figure 2. In vivo volumetric imaging of NTS activity during repeated VNS

(A) Volumetric live imaging of neural activities in the wide brainstem area, including the NTS. Two-photon imaging was performed through the implanted double prism of the head-fixed mouse under anesthesia. The wide field of view and piezo-based z-scanning enabled volumetric imaging of the GCaMP fluorescence.

(B) In vivo NTS imaging was conducted during electrical stimulation of the vagus nerve through a bipolar platinum electrode, which wrapped the cervical vagal trunk in a mouse. The electrode was implanted and fixed with silicone. To create anodal block for efferent direction, cathode (black) and anode (red) were located on rostral and caudal site of vagus nerve, respectively.

(C) Schematic of VNS protocol. In this example, a 1.0 mA, 10 Hz, 100 μs train of electrical stimulation was delivered to the left vagus nerve via an electrode. The term "trial" indicates

a VNS with a pulse width of 100 μs for 10 s, regardless of frequency and current intensity. The term "session" indicates a series of 10-s VNS presentations, with a 90-s interval.

(D) Examples of in vivo volumetric imaging of the NTS. AAVdj/Syn.GCaMP7f was used for this experiment. (Left) As examples, Zp1, 2, and 4, which contain automatically detected ROIs in this mouse, are shown (Zp4 here is the same data as Figure 1G). Median fluorescence over time for each panel is presented in green-fire-blue to show a baseline fluorescence level. (Right) Detection of spontaneous and/or VNS-evoked neural activities (ΔF/F0) from 21 example neurons outside (red) and inside (orange) the NTS. See also Supplementary Movie1.

(E) Higher-magnification imaging provides clear single-cellular precision. AAV1/Syn.GCaMP6f was used for this experiment. (Left) Two-photon imaging utilizes a scanning type observation system, enabling seamless transition from wide-field to high-magnification imaging using a single objective lens. (Right) To clearly distinguish the ROIs by color, median GCaMP fluorescence in the NTS is shown in grayscale. Eleven ROIs, each corresponding to a putative single neuron, are sorted by the magnitude of their responses to the VNS. See also Supplementary Movie2.

Zp, z-stacked horizontal plane obtained by the volumetric scanning. Gray indicates the timing of VNS. D, dorsal; P, posterior; A, anterior; R, right.

Figure. 3

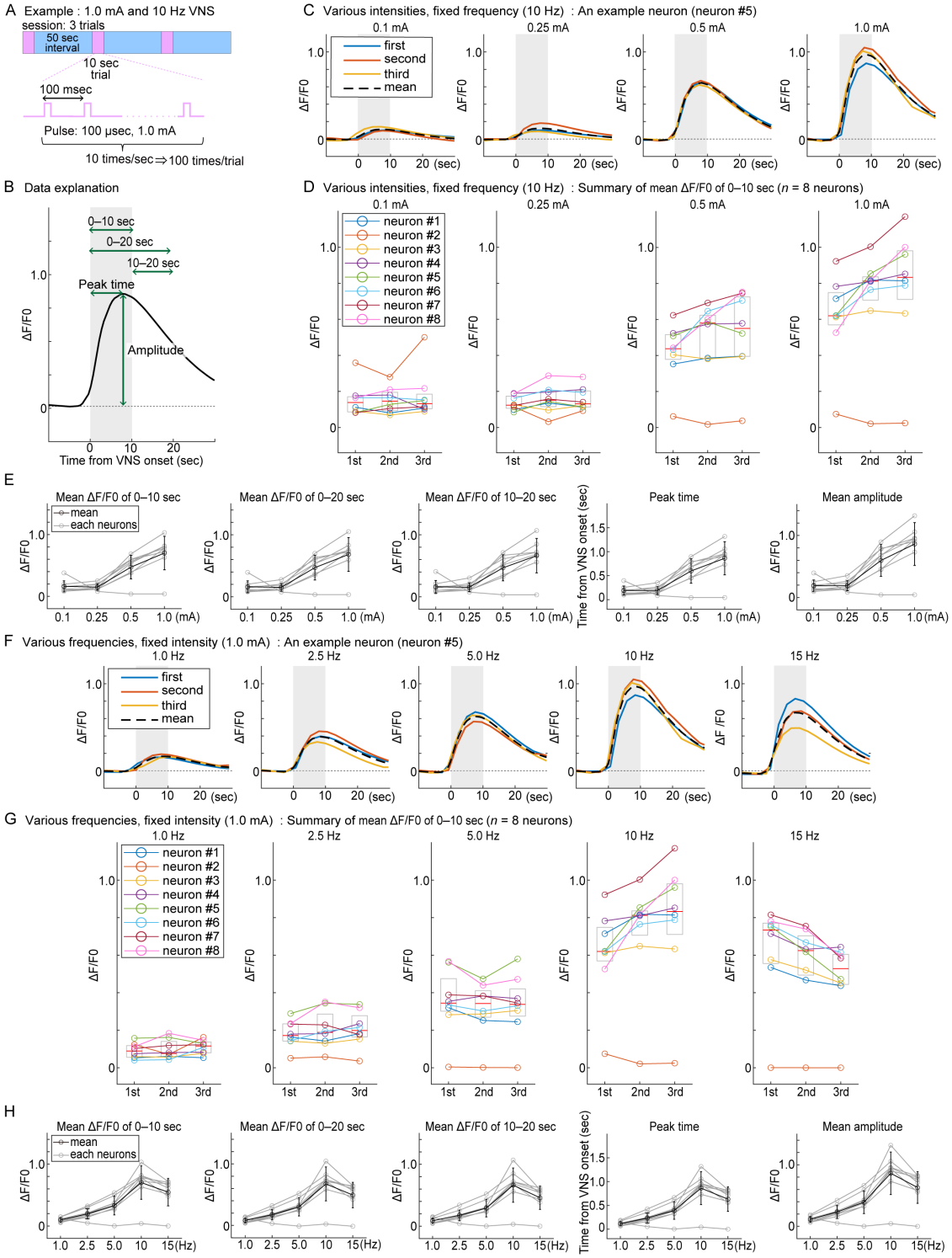

Figure 3. Variable responsiveness of NTS neurons characterized by various VNS conditions

(A) Schematic of VNS protocol. In this example, a 1.0 mA, 10 Hz, 100 μs train of electrical stimulation was delivered. Each experiment in this figure includes a session consisting of

three trials of 10-s VNS presentations, with a 90-sec interval.

(B) Various parameters for evaluating neural responses. The neural response (ΔF/F0) to VNS (gray shaded area), with the horizontal axis representing the time from the VNS onset. Average signal (0−10, 0−20, 10−20 sec), peak time, and amplitude, which are calculated for evaluating neural responses are indicated by green arrows.

(C) Neural responses of an example neuron to VNS at a fixed frequency of 10 Hz, with various stimulus intensities. Colored lines indicate the neural response to the first, second, and third VNS. Dashed line indicates the mean of the responses to three VNSs.

(D) Summary of simultaneously recorded neurons (*n* = 8 neurons in a mouse) to VNS at a fixed frequency of 10 Hz, with various stimulus intensities. The mean ΔF/F0 of each neuron for 10 s from the onset of the VNS at various stimulus intensities are summarized.

(E) Summary of neuronal responses to VNS at a fixed frequency of 10 Hz, with various stimulus intensities. Mean values for three trials, for each neuron or for all neurons, were calculated. Mean ΔF/F0 of 0–10 sec: the mean of ΔF/F0 for 10 sec from the onset of the VNS. Mean ΔF/F0 of 0−20 sec: the mean of ΔF/F0 for 20 sec from the onset of the VNS. Mean ΔF/F0 of 10–20 sec: the mean of ΔF/F0 for 10 sec from the offset of the VNS. Peak time: mean time from the onset of each of the VNS onset to the ΔF/F0 peak. Mean amplitude: mean amplitude of ΔF/F0 within 10 s from the onset of each of the three VNS presentations. Gray lines, response of each neuron; black line, the mean of all neurons.

(F) An example of ΔF/F0 of neuronal responses to VNS at a fixed stimulus intensity of 1.0 mA, with various frequencies. Colored lines indicate the neural response to the first, second, and third VNS. Dashed line indicates mean of the responses to three VNSs.

(G) Summary of simultaneously recorded neurons (n = 8 neurons in a mouse) to VNS at a fixed stimulus intensity of 1.0 mA, with various frequencies. The mean DF/F0 of each neuron for 10 s from the onset of the VNS at various stimulus frequencies are summarized.

(H) Summary of neuronal responses to VNS at a fixed stimulus intensity of 1.0 mA, with various frequencies. Mean values for three trials, for each neuron or for all neurons, were calculated. Mean ΔF/F0 of 0–10 sec, Mean ΔF/F0 of 0–20 sec, Mean ΔF/F0 of 10–20 sec, Peak time, and Mean amplitude were calculated as described in the legend of E. Gray lines, response of each neuron; black line, the mean of all neurons.

AAV1/Syn.GCaMP6s was used for this experiment. Gray shaded are indicates the timing of VNS. Boxes in D and G, 25th–75th percentile; Red bars in D and G, median of all neurons. Error bars in E and H, standard deviation.

1014 **Figure. 4**

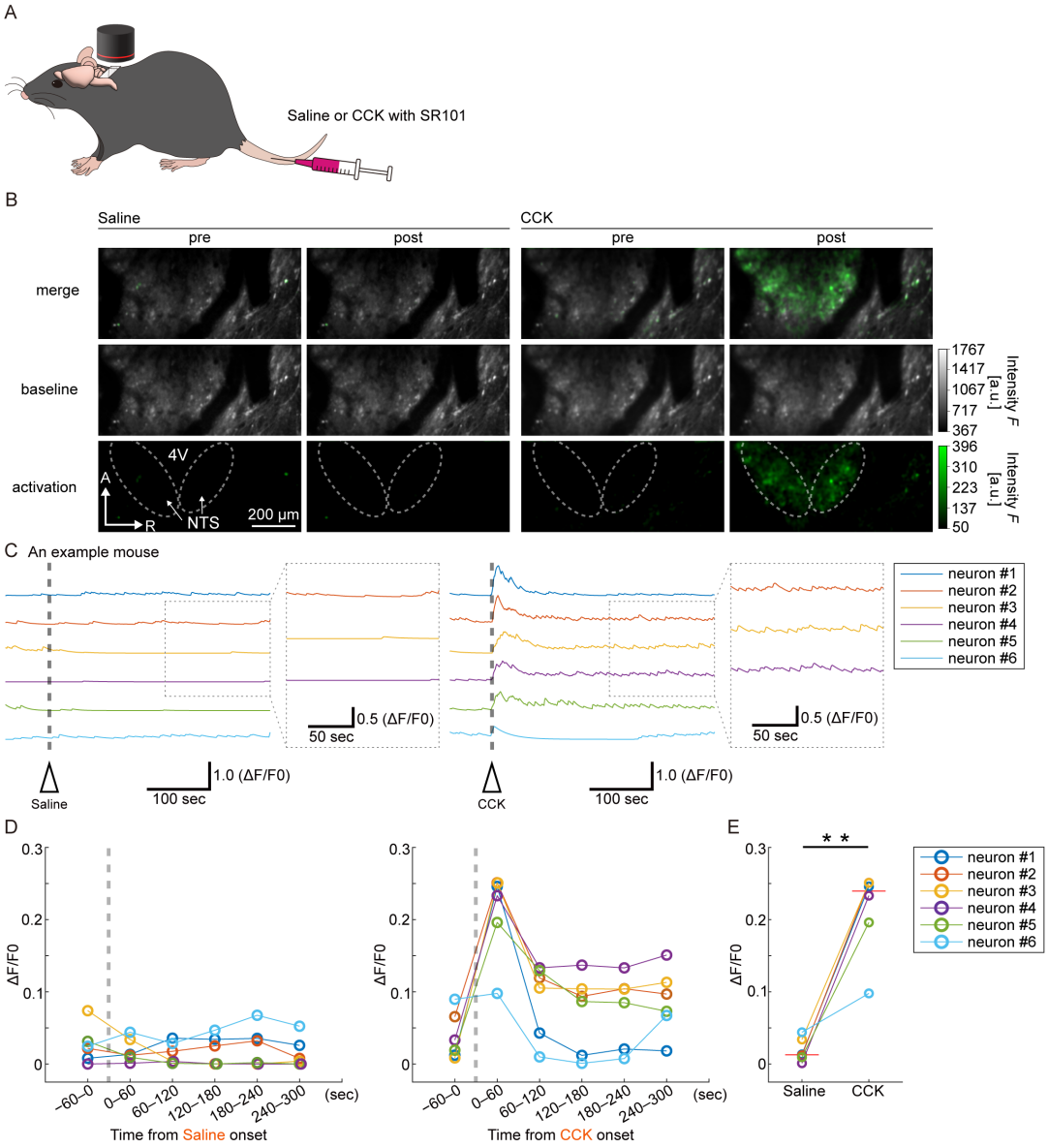

1015

1016 **Figure 4.** Imaging NTS neural activity in response to intravenous CCK administration

1017 (A) Schematic of *in vivo* NTS imaging while CCK and Saline (co-administered with red
1018 fluorescent dye, SR101) were administered into the tail vein of an anesthetized mouse. Note
1019 that CCK administration was performed more than 10 min after saline administration.

1020 (B) Averaged fluorescence of GCaMP signals during pre- and post-administration (60 sec
1021 duration) of Saline or CCK. (Top) Baseline-subtracted signal is shown in green over a
1022 background of the baseline image shown in gray, (middle) baseline fluorescence image,
1023 (bottom) GCaMP signal. Dashed circles indicates the NTS area. 4V, fourth ventricle. See also

1024 Supplementary Movies 4 and 5.

1025 (C) Representative traces of GCaMP fluorescence in simultaneously recorded NTS neurons
1026 (same neurons on the left and right). The timings of respective injections (saline, left; CCK,
1027 right) are indicated by a gray dotted line. Traces regarding more than five minutes after the
1028 injection are expanded to visualize the higher frequency of spontaneous activity uniquely
1029 observed after CCK administration.

1030 (D) The average ΔF/F0 for each 60-sec bin along the time course was calculated for saline (left)
1031 or CCK (right) administration. Each data point represents the mean ΔF/F for each neuron in
1032 each bin.

1033 (E) The boxplot of the average ΔF/F for 60 sec immediately after the administration of saline and
1034 CCK, respectively. Red bars, median of all neurons at each condition (saline and CCK). Red
1035 bars, median of all neurons. $^{**}p < 0.01$, two-tailed Wilcoxon signed-rank test ($p = 0.0011$).

1036 AAVdj/Syn.GCaMP7f was used for this experiment.

1037

Supplementary Materials

Supplementary Materials (Figures. S1 to S6, and caption for Supplementary Movies S1 to S5) are explained in a separate document.

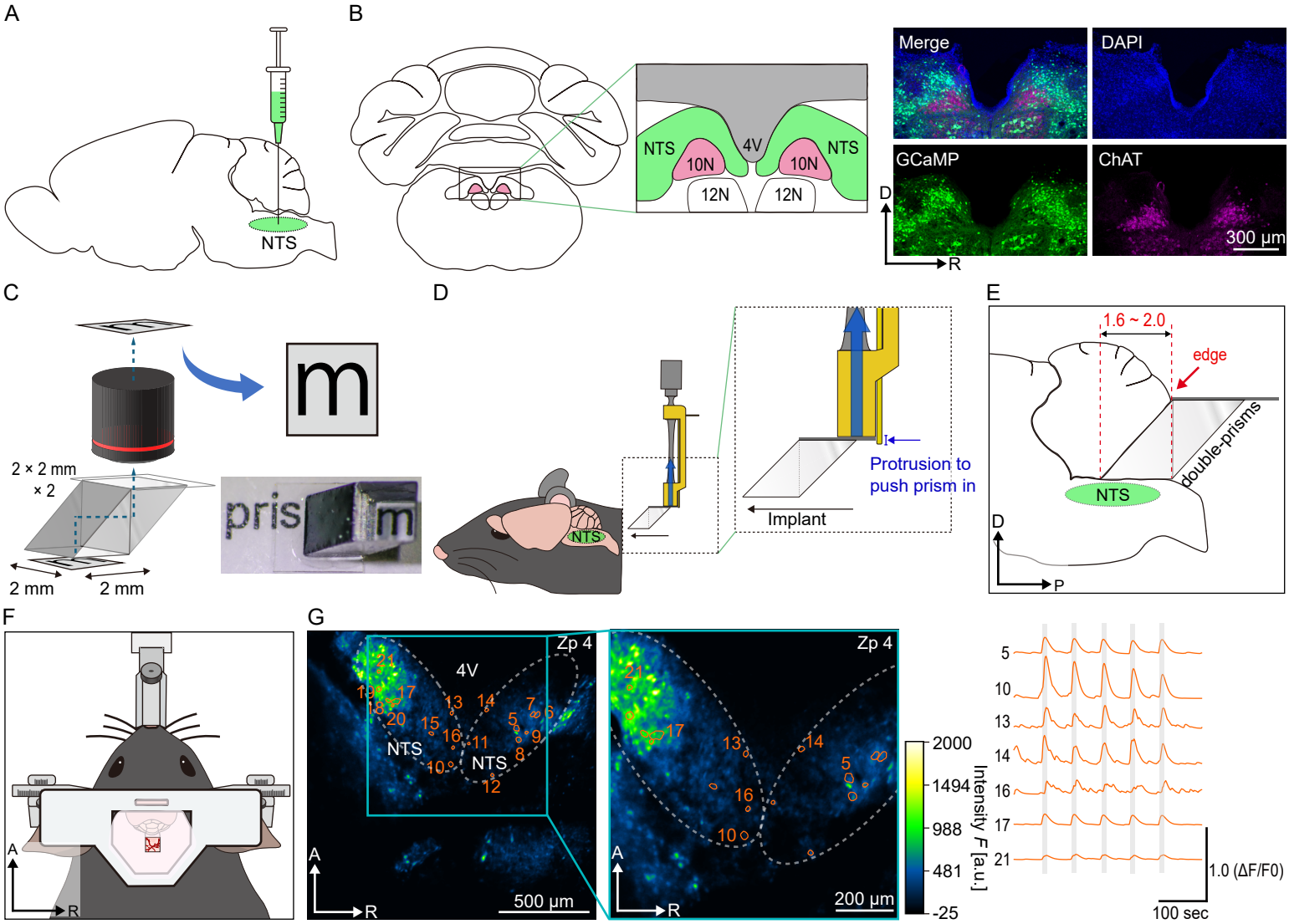
A
NTS
B
NTS
10N
4V
10N
NTS
12N
12N
Merge
DAPI
GCaMP
ChAT
300 μm
D
R
C
2 × 2 mm
× 2
2 mm
2 mm
pris
m
D
NTS
Protrusion to
push prism in
Implant
E
1.6 ~ 2.0
edge
double-prisms
NTS
D
P
F
A
R
G
Zp 4
4V
NTS
NTS
500 μm
Zp 4
200 μm
2000
1494
988
481
-25
Intensity F [a.u.]
5
10
13
14
16
17
21
1.0 (ΔF/F0)
100 sec

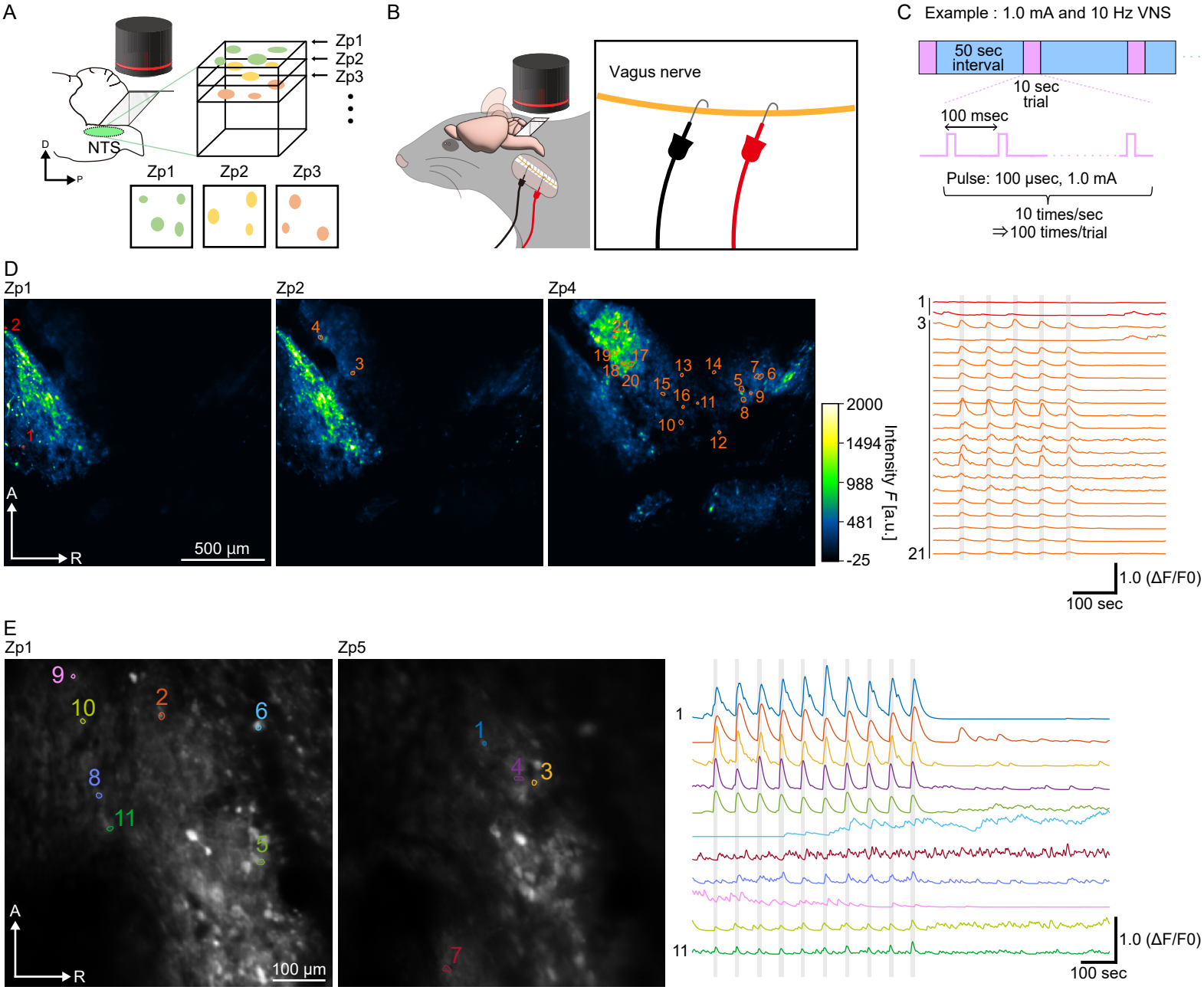
A
Zp1
Zp2
Zp3
NTS
D
P
B
Vagus nerve
C
Example : 1.0 mA and 10 Hz VNS
50 sec interval
10 sec trial
100 msec
Pulse: 100 μsec, 1.0 mA
10 times/sec
⇒100 times/trial
D
Zp1
Zp2
Zp4
A
R
500 μm
2000
1494
988
481
-25
Intensity F [a.u.]
1
3
21
1.0 (ΔF/F0)
100 sec
E
Zp1
Zp5
100 μm
1
11
1.0 (ΔF/F0)
100 sec

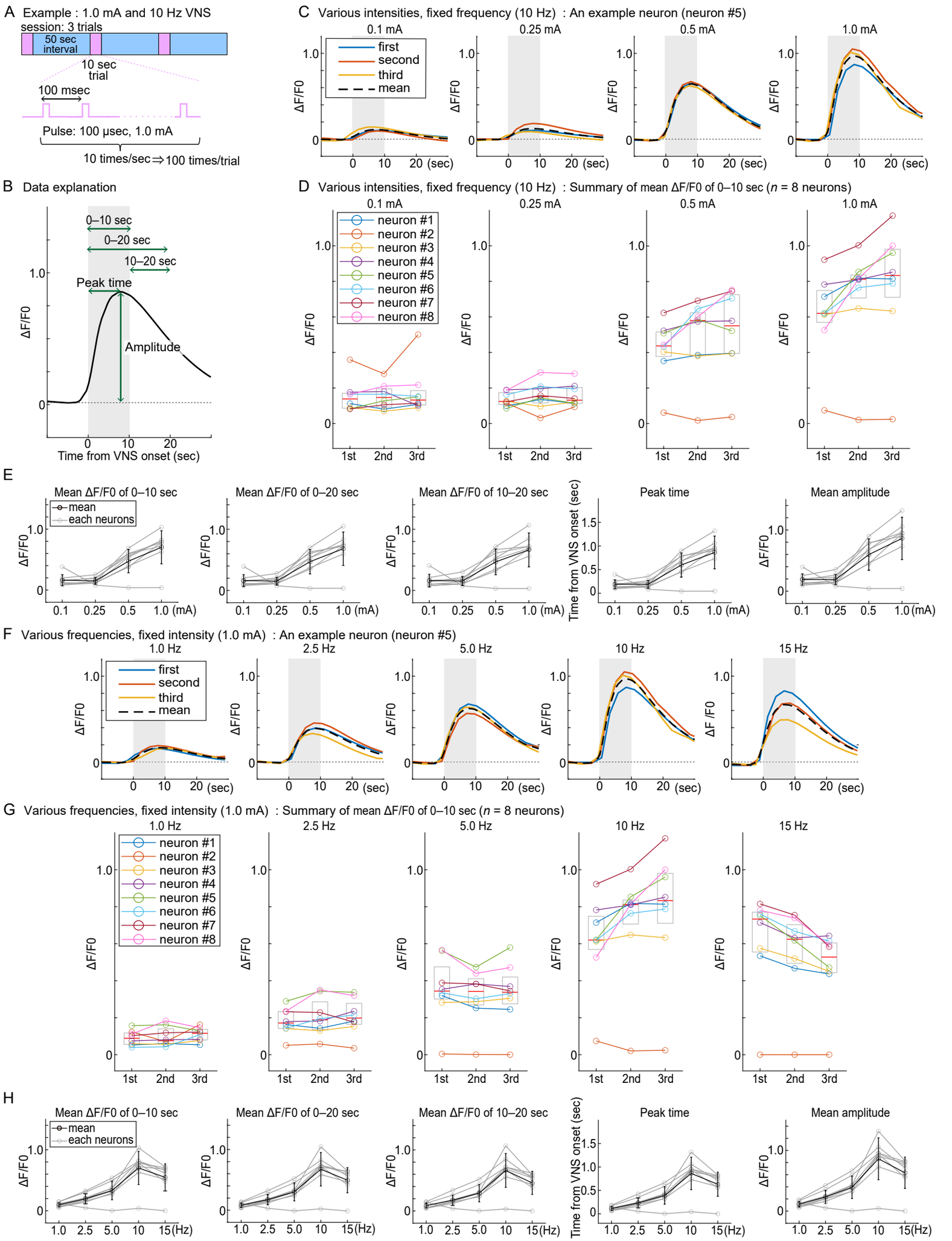
A Example : 1.0 mA and 10 Hz VNS
session: 3 trials
50 sec interval
10 sec trial
100 msec
Pulse: 100 μsec, 1.0 mA
10 times/sec ⇒ 100 times/trial
B Data explanation
0–10 sec
0–20 sec
10–20 sec
Peak time
Amplitude
ΔF/F0
Time from VNS onset (sec)
C Various intensities, fixed frequency (10 Hz) : An example neuron (neuron #5)
0.1 mA
0.25 mA
0.5 mA
1.0 mA
first
second
third
mean
ΔF/F0
(sec)
D Various intensities, fixed frequency (10 Hz) : Summary of mean ΔF/F0 of 0–10 sec (n = 8 neurons)
neuron #1
neuron #2
neuron #3
neuron #4
neuron #5
neuron #6
neuron #7
neuron #8
1st
2nd
3rd
E
Mean ΔF/F0 of 0–10 sec
Mean ΔF/F0 of 0–20 sec
Mean ΔF/F0 of 10–20 sec
Peak time
Mean amplitude
mean
each neurons
Time from VNS onset (sec)
(mA)
F Various frequencies, fixed intensity (1.0 mA) : An example neuron (neuron #5)
1.0 Hz
2.5 Hz
5.0 Hz
10 Hz
15 Hz
G Various frequencies, fixed intensity (1.0 mA) : Summary of mean ΔF/F0 of 0–10 sec (n = 8 neurons)
H
(Hz)

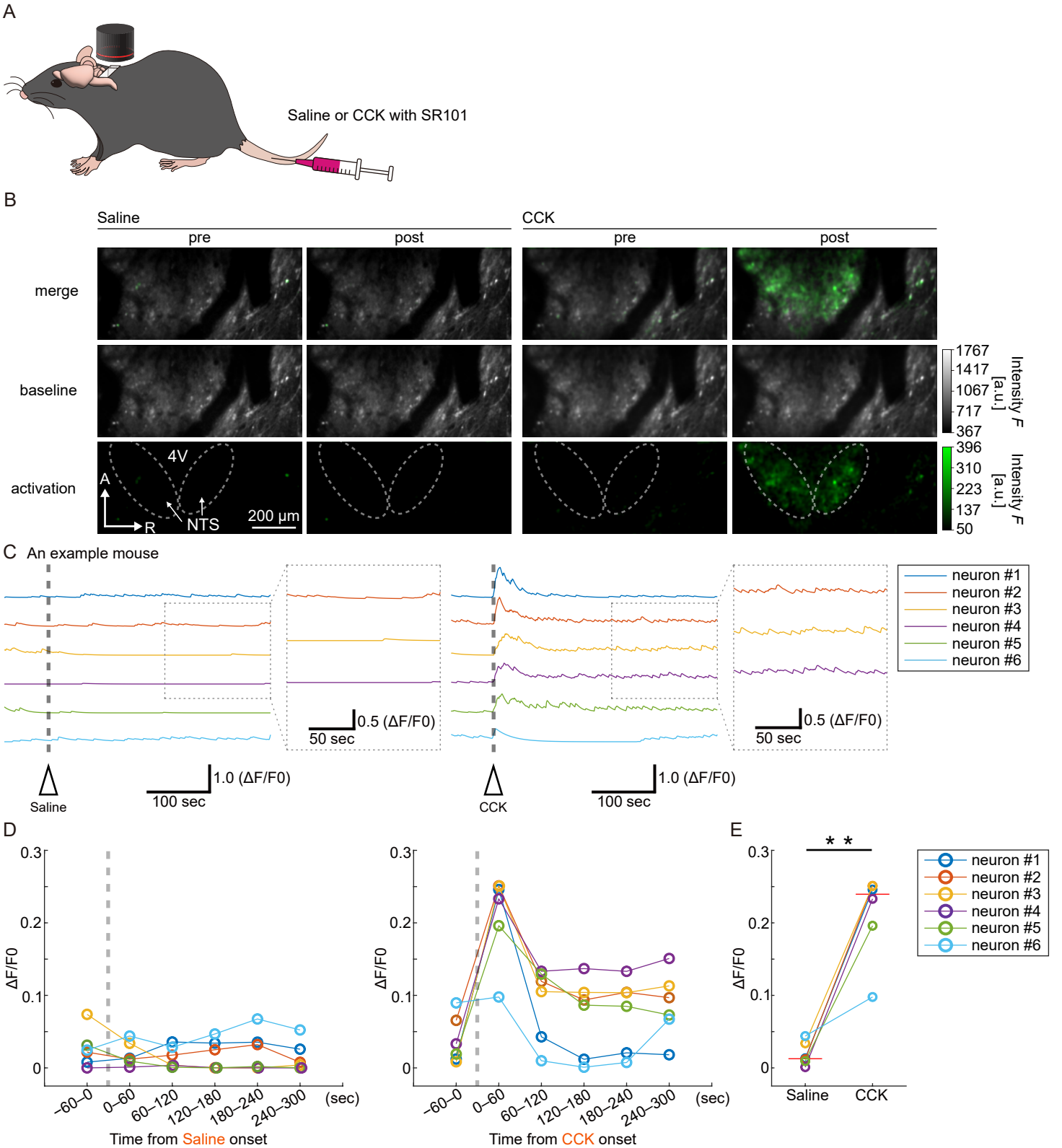
A
Saline or CCK with SR101
B
Saline
CCK
pre
post
merge
baseline
activation
4V
A
R
NTS
200 μm
1767
1417
1067
717
367
Intensity F [a.u.]
396
310
223
137
50
Intensity F [a.u.]
C An example mouse
neuron #1
neuron #2
neuron #3
neuron #4
neuron #5
neuron #6
0.5 (ΔF/F0)
50 sec
1.0 (ΔF/F0)
100 sec
Saline
CCK
D
ΔF/F0
0.3
0.2
0.1
0
−60–0
0–60
60–120
120–180
180–240
240–300
(sec)
Time from Saline onset
Time from CCK onset
E
* *
Saline
CCK